water

Article

Geothermometry and Isotope Geochemistry of CO$_2$-Rich Thermal Waters in Choygan, East Tuva, Russia

Anastasia Shestakova [1],* , **Natalia Guseva [1]**, **Yulia Kopylova [1]**, **Albina Khvaschevskaya [1]**, **David A. Polya [2] and Igor Tokarev [3]**

[1] Research and Education Centre "Water", National Research Tomsk Polytechnic University, 30 Lenin Avenue, Tomsk 634050, Russia; guseva24@yandex.ru (N.G.); unpc_voda@mail.ru (Y.K.); garibova@yandex.ru (A.K.)

[2] School of Earth and Environmental Science and Williamson Research Centre for Molecular Environmental Science, University of Manchester, Manchester M13 9PL, UK; david.polya@manchester.ac.uk

[3] Resource center "Geomodel", Research Park of Saint-Petersburg State University, Ulyanovskvayast. 1, Saint Petersburg 198504, Russia; tokarevigor@gmail.com

* Correspondence: ashest91@mail.ru; Tel.: +7-909-540-4503

Abstract: The Choygan area of southern Siberia, Russia hosts a variety of CO$_2$-rich thermal mineral and other waters emerging from springs at temperatures between 7 °C and 39 °C. Chemical analyses of the spring waters (n = 33) were carried out to characterise the waters and determine their origin. A continuum of compositions was observed between relatively lower temperature (7 °C) HCO$_3$-Ca-Na dominated waters with relatively low amount of total dissolved solids (TDS) and high Eh, and higher temperature (39 °C) HCO$_3$-Na-Ca dominated waters with higher TDS and lower Eh—this reflects largely conservative mixing of these components between near surface low temperature, oxidising groundwaters and higher temperature, more reducing thermal waters derived from a deeper geothermal reservoir. Stable isotopic data are consistent with all the water ultimately being derived from meteoric water that has undergone varying degrees of isotopic fractionation following evaporation. The inferred δ^{18}O and δ^{2}H isotopic composition of the unfractionationed meteoric waters is lighter than that expected that of mean annual local precipitation, which together with a strong negative correlation between δ^{18}O and the elevation of the sampled discharging springs, suggests recharge at higher elevations (1600 m to 3000 m; average 2600 m). Reservoir temperature, calculated using geothermometers and an analysis of saturation indices of plausible reservoir minerals, ranged from 70 °C to 100 °C at an inferred depth of 2 to 3 km. Not all chemical components were found to follow conservative mixing behaviour. In particular, (i) the CO$_2$ contents of the waters were highly variable, suggesting either varying degrees of degassing and/or near discharge admixture with air, and (ii) SO$_4$ concentrations in the lower temperature thermal CO$_2$-rich waters were highly variable, suggesting a role of near surface oxidation processes, for example of pyrite, in modifying the concentration of redox sensitive components. Limited δ^{13}C data are consistent with the CO$_2$ predominately being derived from dissolution of metamorphic/igneous carbonate minerals in the reservoir. Based on geological conditions, isotope and chemical data, a conceptual circulation model of the Choygan hydrothermal system is proposed.

1. Introduction

One current challenge in geochemistry is determining the genesis and particularly the geochemical processes controlling the chemical compositions of mineral waters, which are often generated in complex hydrogeological systems. These waters, particularly carbon dioxide-rich mineral waters, are widely used for a variety of purposes including geothermal power, carbon dioxide production, heating of shelters and greenhouses as well as bottled water and spas. Better understanding their origins may be helpful to inform sustainable development of these resources.

Mineral water springs are typically located in tectonically active areasandare frequently associated with fracture zones [1]. Well known examples are recorded in Turkey [2,3], Iran [1,4], Serbia [5,6], Tunisia [7,8], Mexico [9,10], China [11,12], Korea [13–15], Portugal [16,17], Spain [18], Italy [19], France [20,21], Egypt [22,23] and Russia [24,25] amongst other places.

The Choygan mineral water spa, used for several decades by locals and tourists for bathing and medicinal purposes, is an example of such an occurrence of carbon dioxide-rich mineral waters. Located in the Eastern Sayan Mountains, Tuva, Russia, some of these springs are characterized by the bubbling of CO_2-rich gases. Our group [26,27] have determined the dissolved gas [26], ^{222}Rn [26] and major and trace chemical compositions of these waters [28,29] (see also previous work summarized in [26,27] as well as making an assessment of the extent of thermodynamic equilibrium of these waters with various minerals [26]). These have enabled preliminary estimates of reservoir temperatures [30,31]. Further constraints on the origins of these waters have been provided by ^{3}He/^{4}He based heat flow estimates [32]. Notwithstanding these studies, the difficulty of access has precluded more detailed studies of these mineral waters, in particular in relation to geothermometry, isotope geochemistry and the application of these techniques to developing a more detailed conceptual model of the origins of the mineral waters.

This study aims to conduct a more detailed survey of the Choygan CO_2-rich thermal waters and to better define the geological and geochemical conditions of formation of the mineral waters and, in particular, the extent and nature of water–rock reaction processes (cf. [1,3,33]). We apply hydrogeochemical geothermometers [4,9,22] to establish the maximum reservoir temperatures, ascertain the effect of CO_2 and temperature on the main processes that control the water chemistry and to estimate the depth of the geothermal system (cf. [4,9,22]). We use stable isotopes (δ^{18}O and δ^2H) to provenance the waters (cf., [1,26]) and to better understand underground flow paths. Lastly, this study aims to provide an improved conceptual circulation model of the Choygan hydrothermal system.

2. Study Area

The Choygan mineral water natural spa is located in the northeastern part of the Tuva Republic (Russia) at a height of around 1550 m and in an area characterized by a continental climate, a mean annual temperature −4.7 °C with an annual average precipitation of 700 mm (Figure 1) [34]. The groundwaters discharge at 33 local springs within a relatively small area on the western slope of the Eastern Sayan Mountains (Figure 2). The springs are predominantly located on the right bank of the Arzhaan–Hem River, on the first river terraces along the slope as well as in the floodplain of the left riverbank.The combined total discharge from all of the springs is estimated to be around 18 L/s.
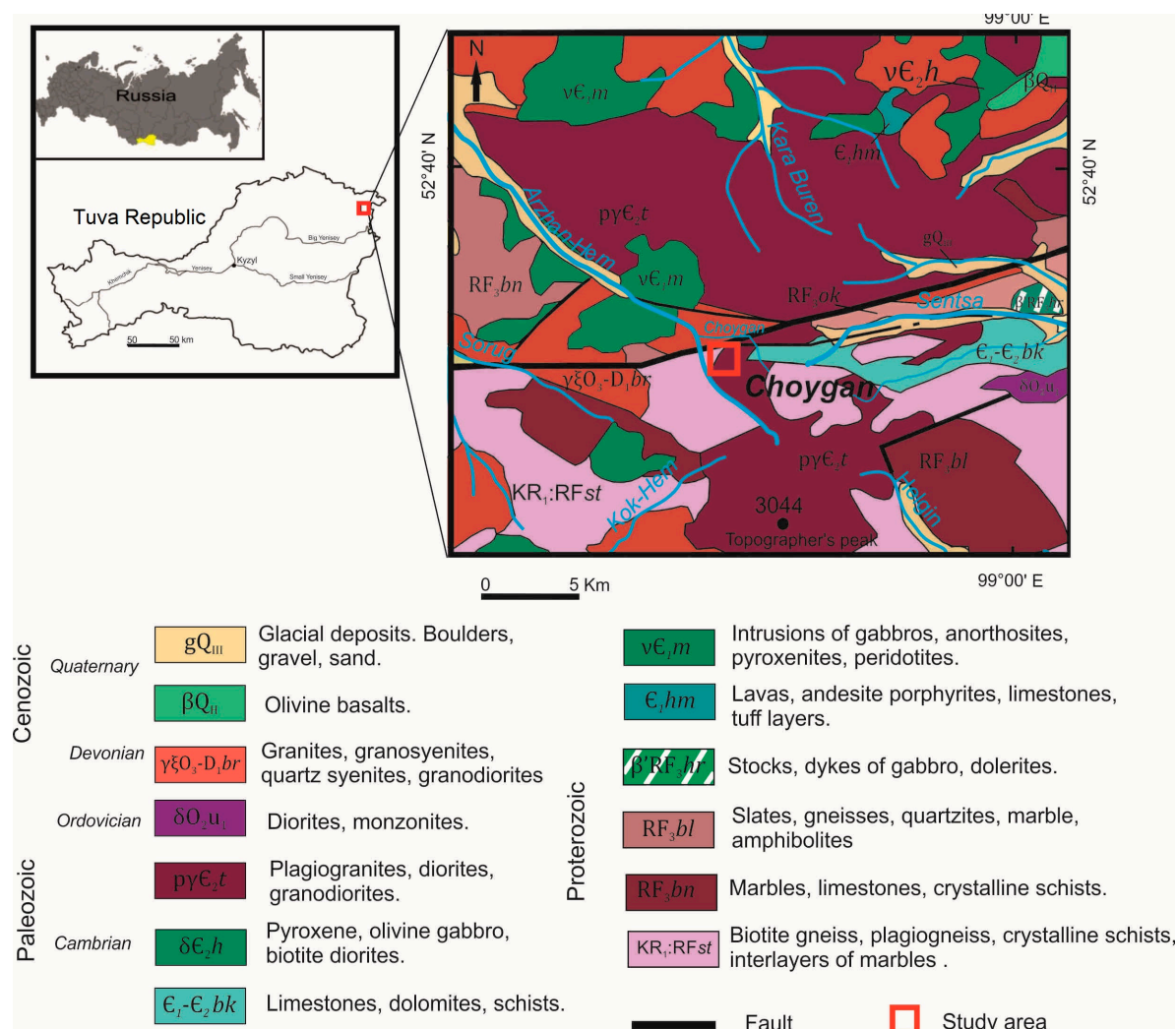
Figure 1. Location and geological setting of the study area (the square indicates the sampling field; for the sampling point locations, see Figure 2) [35].

The Choygan springs lie at the boundary of the Riphean Tuva–Mongolian massif with older Caledonian structures of the Eastern Tuva. The springs are located at the intersection of the topographic low due to the Arzhan-Hem river and the zone of the deep E-W trending Azassko–Zhomboloksky fault. The springs emerge in Lower Paleozoic intrusives on the right bank of the Arzhan–Hem River and crystalline schists, gneisses and marbles on the left bank (Figure 1). The Eastern Sayan Mountains, in which the Choygan springs are located, are characterized by high seismic activity and young volcanoes. A small field of the Cenozoic basalts is situated 20 km northeast of the Choygan springs.

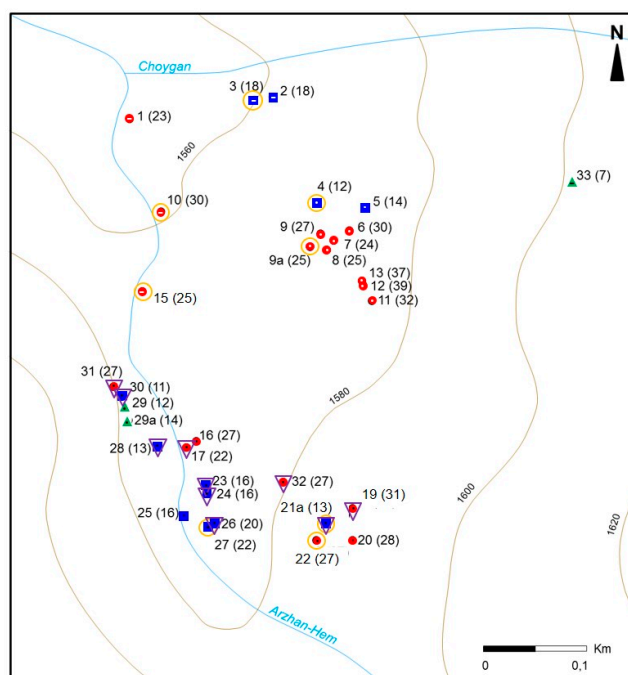**Figure 2.** Location of sampling points in the Choygan field. Temperatures (°C) of spring water given in parentheses. Red closed circle—higher temperature thermal CO_2-rich waters, blue close square—lower temperature thermal CO_2-rich waters, green triangle—shallow groundwater; an open yellow circle shows $CO_2 > 35$ vol.%; an open purple diamond—$SO_4 > 0.4$ meq/L. Grouping of samples based on a geographical location on study area:white dots—group of samples 4, 5, 6, 7, 8, 9, 9a, 11, 12, 13; black dots—group of samples 16, 17, 19, 20, 21a, 22, 23, 24, 25, 26, 27, 28, 29, 29a, 30, 31, 32; white dash—group of samples 1, 2, 3, 10, 15; black dash—spring 33.

3. Materials and Methods

Water samples (*n* = 33) including those from both higher temperature (T > 23 °C) and lower temperature (T < 23 °C) springs were collected in July 2013. Samples for analysis for ion chromatography or titrimetric analysis were collected in 500-mL clean polyethylene bottles after rinsing twice with the sampled water. The samples for trace element analyses were acidified with concentrated HNO_3 to prevent metal precipitation and stored in 50-mL clean polyethylene bottles. Spring temperature, pH, Eh and electric conductivity (EC) were measured in situ using a portable water test kit (Hanna Instruments, Vöhringen, Germany). In addition, dissolved CO_2 was measured in the field by titration with NaOH.

The concentration of HCO_3^- was estimated via titration with a 0.01 M solution of HCl using a methyl orange indicator. Ions, including SO_4^{2-}, Cl^-, Ca^{2+}, Mg^{2+}, Na^+ and K^+, were analysed using ion chromatography (Dionex 1000 and Dionex 2000). Dissolved trace elements were determined by inductively coupled mass spectrometry (Perkin Elmer Inc., ELAN-DRC-e, Shelton, CT, USA). All standard solutions for these analyses were prepared with ultra-pure deionized water and Perkin Elmer Multi Element Standard Solutions. Ionic charge balance was calculated and used as a quality control check. The value of the computed ionic charge balance was within an acceptable limit of ±5% for most samples.

The radon content of the water samples was determined using a radiometer RGA-01 (Allbiz, Zelenograd, Russia), which registered the volume alpha-radiation activity of the radon-222 nuclide in liquid samples.

Gas samples (*n* = 26) were taken via the vacuum method at the field temperature in 0.2–L glass bottles using a portable syringe-degasser [36]. The composition of the dissolved gas (N_2, O_2, CO_2)

was determined with a Chromatec Crystal-2000M chromatograph using Chromatec Analyst software (version 3.0, JSC "Chromatec", Yoshkar-Ola, Russia).

The analysis of the chemical and gas compositions of the waters was performed at the Laboratory of Hydrogeochemistry of the "Voda" (Water) Research Centre of the Institute of Natural Resources at Tomsk Polytechnic University.

Water $\delta^{18}O$ and δ^2H ($n = 19$) were analysed at the Resource Centre 'Geomodel' Research Park of Saint-Petersburg State University (St. Petersburg, Russia) on a Picarro L-2120i laser spectrometer (Picarro Inc., Santa Clara, CA, USA). V-SMOW-2, GISP, SLAP, USGS45 and USGS46 were used as standards. Accuracy is estimated to be better than $\pm 0.1\%$ for $\delta^{18}O$ and $\pm 1\%$ for δ^2H. A limited number of further samples were analysed for $\delta^{13}C$ at the Laboratory of Isotope and Analytical geochemistry (Novosibirsk, Russia).

Silica (quartz and chalcedony) and cation (Na–K–Ca and Na–K) geothermometers were used to estimate the reservoir temperatures of the Choygan geothermal system using the chemical analyses of the thermal waters (Table 1) using the equations as follows:

Quartz geothermometer (Fournier and Potter, 1982) [37]:

$$T = -42.198 + 0.278831S - 3.668 \times 10^{-4} - 4S^2 + 3.1665 \times 10^{-7}S^3 + 77.034 \log S \tag{1}$$

Chalcedony geothermometer (Fournier, 1977) [37]:

$$T = \frac{1309}{5.19 - \log S} - 273.15 \tag{2}$$

Na–K–Ca geothermometer (Fournier and Truesdell, 1973) [37]:

$$T = \frac{1647}{(\log \frac{Na}{K} + \beta \log \frac{Ca^{0.5}}{Na} + 2.06) + 2.47} - 273.15, \qquad \beta = \frac{4}{3} \text{ for } T < 100°C \tag{3}$$

Na–K geothermometer (Truesdell, 1976) [37]:

$$T = \frac{856}{0.857 + \log \frac{Na}{K}} - 273.15 \tag{4}$$

Na–K geothermometer (Fournier, 1979) [37]:

$$T = \frac{1217}{1.483 + \log \frac{Na}{K}} - 273.15 \tag{5}$$

Na–K geothermometer (Arnorsson et al., 1983b) [37]:

$$T = \frac{933}{0.933 + \log \frac{Na}{K}} - 273.15 \tag{6}$$

where T is the model reservoir temperature in °C; S is the silica concentration of the spring discharge in mg/L; and Na, K and Ca concentrations are expressed in mol/L [37].

The depth of origin of the thermal waters was calculated using the following equation:

$$h = \frac{T - T_s}{\gamma}, \tag{7}$$

where T is the model reservoir temperature in °C, T_s is the annual mean surface temperature in °C, and γ is the reported regional geothermal gradient in °C/km.

In the absence of reservoir rock samples, mineral equilibrium calculations, through geothermometry or calculation of saturation indices (SI), are important methods to assess likely

reactive minerals in the subsurface from groundwater chemical data [3]. Mineral saturation indices (SI) for some key carbonate (calcite, aragonite and dolomite), silicate (albite, muscovite and kaolinite), sulphate (gypsum and anhydrite) and silica (quartz and chalcedony) minerals were used to predict the tendency for precipitation or dissolution of those minerals with SI = 0 indicating thermodynamic equilibrium; SI > 0 indicating oversaturation, and SI < 0 indicating undersaturation. Mineral saturation indices of waters from the study area were calculated at the in situ measured spring temperatures and pH using the computer program PHREEQC (version 3, USGS, Denver, CO, USA). The Geochemist's Workbench program (GWB) [38] (Aqueous Solutions LLC, Alexandria, VA, USA) was used to plot activity diagrams.

Following the method of Reed and Spycher (1984) [39], the congruence of mineral saturation indices of potential reservoir minerals over a range of pCO_2 (calculated using Henry's Law and the CO_2 concentrations in the water) and temperatures was used to better estimate reservoir temperatures. The median (RMED), mean (MEAN), standard deviation (SDEV) and root mean-square error (RMSE) of the saturation indices of 9 selected potential reservoir minerals were determined for temperatures between 10 °C and 200 °C and the minimum values of these parameters then used to infer a model most probable reservoir temperature. In order to avoid biases arising from using the saturation indices of minerals with slow reaction kinetics, the median (RMED) was the preferred statistical parameter used to compute reservoir temperature, with SDEV or RMSE used to independently estimate the quality of clustering of saturation indices [39,40].

4. Resultsand Discussion

4.1. Hydrogeochemical Characteristics of the Springs

The major ion chemical compositions of the spring water samples are presented in Table 1 and plotted in a Piper diagram (Figure 3). The spring waters have been grouped into (I) "Higher" temperature (T > 23 °C) thermal CO_2-rich waters; (II) "Lower" temperature (T < 23 °C) thermal CO_2-rich waters; and (III) shallow (non-thermal) groundwaters. Data from our group [26] for samples previously collected from the same area in 2011 are also included for comparison. Chemical compositional difference between waters sampled in 2011 [26] and 2013 (this study) were generally insignificant or small, with observed differences in TDS of typically just 10–200 mg/L, fluorine (0.1–0.9 mg/L) and iron (0.1–1 mg/L); however, larger differences in TDS (400–500 mg/L) were observed in several springs, perhaps reflecting changes in weather and hydrological conditions impacting on mixing between groundwaters of whatever type and rainwater [41].

The first group of 18 relatively high temperature (22 °C to 39 °C) thermal springs is located in the central part of the river floodplain, including that on the left river bank. These waters are characterized by low Eh (−170 V to 142 mV). These "higher temperature" thermal CO_2-rich waters are HCO_3–Na–Ca type, slightly acidic (pH 6.1–6.9) waters with TDS from 1545 mg/L to 2647 mg/L. The TDS values and concentrations of major ions such as HCO_3^-, Cl^-, Ca^{2+}, Na^+, Mg^{2+}, K^+ and Si^{4+} increase with measured water temperature and are higher than those in the colder springs. This likely reflects, in part, longer circulation and residence times of the higher temperature water, with HCO_3 ultimately derived from the dissolution of carbonate minerals and of CO_2, and Na^+, K^+, Ca^{2+}, and Si^{4+} in groundwater associated with the dissolution of silicate phases in the subsurface [3,33]. The coating of a red precipitate around the springs is a result of the oxidation of Fe^{II} to Fe^{III} upon exposure to the atmosphere. This iron may have been leached from biotite and pyroxenes contained in gneisses and crystalline schists in the subsurface.
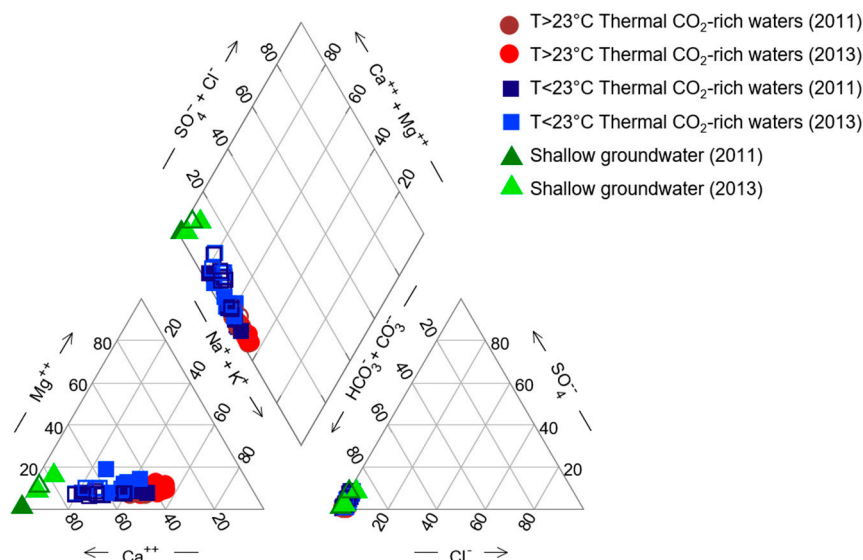
Figure 3. Piper diagram of spring water compositions in the study area (data for 2011 [26], 2013 this study). Open symbols are samples with $SO_4 > 0.4$ meq/L.

The second group of 12 relatively low temperature thermal CO_2-rich waters found in the northeast and southwest parts of the study area are of the HCO_3–Ca–Na type.These waters are slightly acidic (pH 5.9 to 6.7) and with relatively high Eh (170 mV to 236 mV). In contrast to the first group, the TDS values of the second group are relatively low, ranging from 607 to 2064 mg/L, whereas the CO_2 concentration reaches 1488 mg/L with an average of 817 mg/L. The higher CO_2 values may reflect, in part, the higher solubility of CO_2 at lower temperatures. The low Fe (0.1–0.2 mg/L) compared to the "higher temperature" thermal waters (0.1–4.4 mg/L) and relatively high concentration of SO_4^{2-} (5–59 mg/L) in the low temperature water are both consistent with the relatively oxidizing Eh conditions in this group of springs. K and Mg are found in low concentrations in both the higher and lower temperature thermal waters corresponding to their low content in the metamorphic bedrocks.

The discharge of shallow groundwater is represented by three springs situated on the left riverbank and on the slopes of the right bank. This group of HCO_3–Ca type waters shows that the lowest discharge temperatures (7 °C to 14 °C) is circumneutral/weakly alkaline (pH 6.6–8.3) with relatively high Eh (169 mV to 224 mV) and low TDS (290 to 350 mg/L), these low values being consistent with low levels of water–rock interactions. The observed discharge temperatures of these Group III waters are consistent, assuming a plausible local geothermal gradient of 33 °C/km [32], with conductive heating at depths of between 0 and 400 m of waters of meteoric origin and with recharge temperatures between 0 °C and average daily maximum air temperatures of around 13 °C. Notwithstanding this, some mixing with thermal waters cannot be discounted.

The relationship between various chemical constituents and the conservative tracer [1,42], Cl^-, in the three groups of waters are presented in Figure 4. The strong positive correlations between all of Na^+, Mg^{2+}, K^+ and HCO_3^- with Cl^-, is broadly consistent with the major element chemistry being controlled by mixing between a higher temperature thermal CO_2-rich water (cf. Group I) and lower temperature shallow groundwater (cf. Group III)— indeed, with the notably exception of SO_4^{2-}, the major element compositions of the lower temperature thermal CO_2-rich waters (Group II) are generally intermediate between those of Group I and Group III, and those of all the waters generally intermediate between the compositions of Spring 10 and Spring 33, which represent the observed extreme compositional end-members of Group I and Group III respectively. Notwithstanding this, Ca^{2+} is somewhat less correlated with Cl^-, suggesting that its variation is also controlled to some degree by variable dissolution of carbonate minerals and degassing of CO_2, which in turn controls

HCO_3^- concentrations. Several samples also exhibit relatively elevated SO_4^{2-} due to a different process, possibly the oxidation of iron sulphide minerals, such as pyrite.
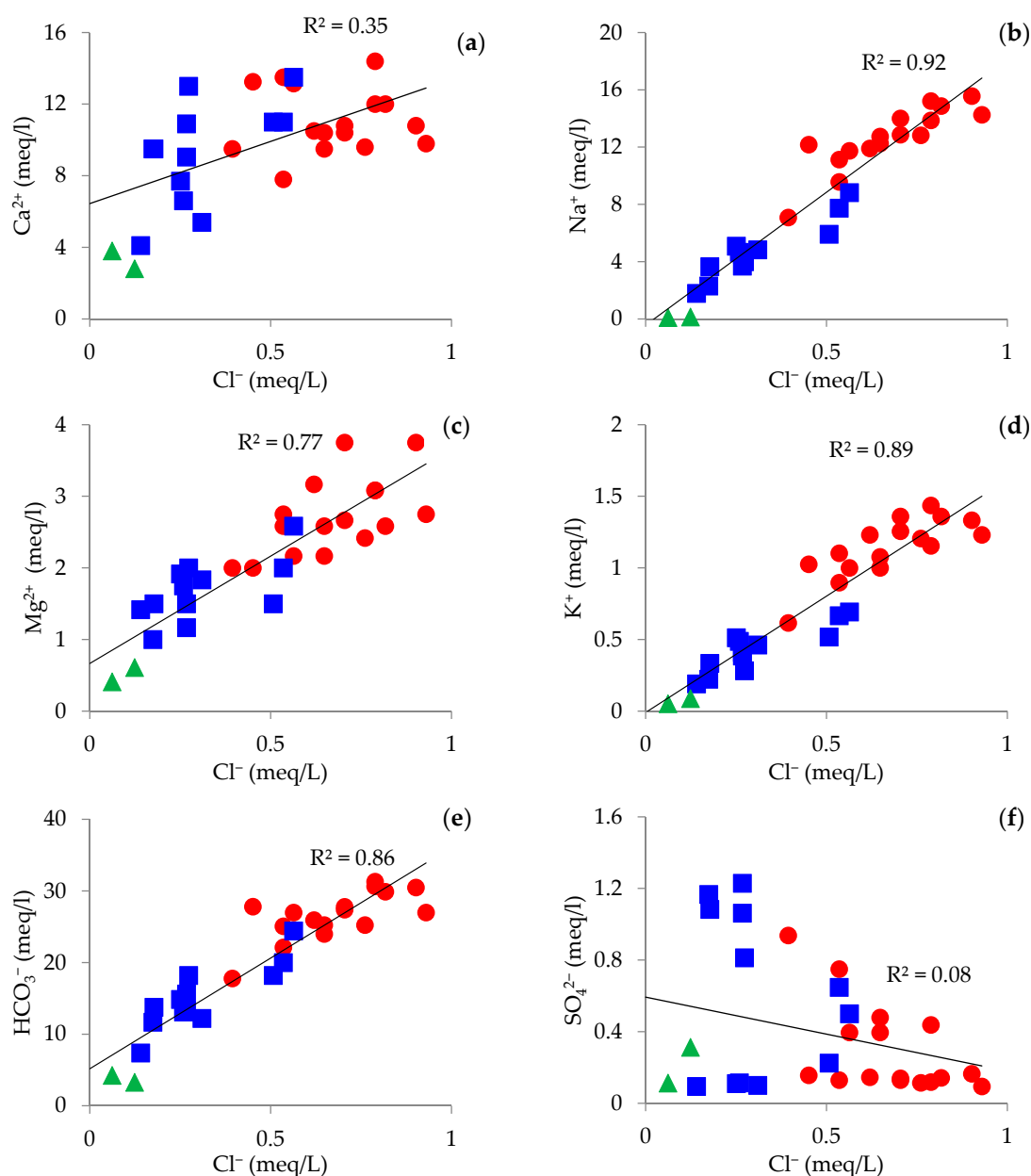

Figure 4. (**a**) Ca^{2+}, (**b**) Na^+, (**c**) Mg^{2+}, (**d**) K^+, (**e**) HCO_3^-, and (**f**) SO_4^{2-} (in meq/L) vs. Cl (in meq/L) binary diagrams for the Choygan spring waters. The symbols are the same as for Figure 3.

Table 1. Chemical, gas and isotopic compositions of Choygan spring waters. For each location number, the top line refers to sample collected in 2013 (this study) and the bottom line for samples collected in 2011 [26] (n.d. indicates no data).

Loc. No	T (°C)	pH	TDS [a] (mg/L)	Eh (mV)	HCO_3^- (mg/L)	SO_4^{2-} (mg/L)	Cl^- (mg/L)	Ca^{2+} (mg/L)	Mg^{2+} (mg/L)	Na^+ (mg/L)	K^+ (mg/L)	Fe (mg/L)	SiO_2 (mg/L)	CO_2 [b] (mg/L)	F (mg/L)	O_2 (vol.%)	N_2 (vol.%)	CO_2 (vol.%)	N_2/O_2 (mol/mol)	^{222}Rn [c] (Bq/L)	$\delta^{18}O$ (%SMOW [d])	δ^2H (%SMOW [d])
									Higher temperature (T > 23 °C) thermal CO_2-rich waters													
1	23 [e]	6.2	2288	62	1646	4.5	33	196	33	328	48	1.5	50	1133	0.3	n.d.	n.d.	n.d.	n.d.	n.d.-	−14.4	−132
	25 [f]	6.5	2097	46	1537	5.4	19	180	27	282	46	2.5	53	356	1.1	n.d.	n.d.	n.d.	n.d.	123	n.d.	n.d.
6	30 [e]	6.3	2332	−90	1695	6.2	25	216	45	296	49	2.1	50	744	0.2	15	58	27	3.9	95	−17.3	−138
	31 [f]	6.4	2420	34	1757	12	17	276	25	287	46	1.7	46	407	1.1	n.d.	n.d.	n.d.	n.d.	370	n.d.	n.d.
7	24 [e]	6.4	1863	−150	1350	6.2	19	156	33	256	43	0.7	43	800	0.1	16	62	22	3.9	n.d.	−15.2	−130
	21 [f]	6.4	2368	−86	1732	9.1	16	276	25	280	42	0.3	38	371	0.9	n.d.	n.d.	n.d.	n.d.	204	n.d.	n.d.
8	25 [e]	6.3	2328	−170	1696	7.5	16	265	24	280	40	1.1	49	277	n.d.	14	58	28	4.1	n.d.	n.d.	n.d.
	22 [f]	6.3	2353	−68	1696	7.5	16	265	24	280	40	0.2	41	277	1.0	n.d.	n.d.	n.d.	n.d.	360	n.d.	n.d.
9	27 [e]	6.2	2180	−24	1582	7.0	22	210	38	274	48	0.5	45	371	0.3	17	65	18	3.8	n.d.	n.d.	n.d.
	28 [f]	6.8	2302	12	1692	11	18	290	25	251	40	0.5	43	352	0.9	n.d.	n.d.	n.d.	n.d.	947	n.d.	n.d.
9a [f]	25 [f]	6.9	2136	22	1540	5.5	27	192	29	295	47	n.d.	n.d.	409	0.3	10	48	42	4.8	84	−15.9	−134
10	30 [e]	6.5	2570	21	1860	7.9	32	216	45	358	52	1.3	55	460	0.7	9	37	55	n.d.	n.d.	n.d.	n.d.
	31 [f]	6.5	2712	24	1970	10	34	284	34	348	54	1.6	50	496	1.2	n.d.	n.d.	n.d.	n.d.	64	n.d.	n.d.
11	32 [e]	6.3	2318	29	1671	6.7	25	208	32	322	53	0.4	47	746	1.1	12	52	36	4.3	n.d.	−18.6	−143
	29 [f]	6.5	2413	86	1732	10	21	266	26	303	45	0.4	44	349	1.0	n.d.	n.d.	n.d.	n.d.	310	n.d.	n.d.
12	39 [e]	6.3	2525	−54	1824	6.8	29	240	31	342	53	1.2	50	691	0.5	15	58	27	4.8	n.d.	−18.4	−142
	37 [f]	6.6	2515	55	1830	8.5	23	275	30	312	50	1.3	54	333	1.2	n.d.	n.d.	n.d.	n.d.	139	n.d.	n.d.
13	37 [e]	6.3	2586	20	1870	5.7	28	240	37	350	56	1.3	51	613	1.1	n.d.	n.d.	n.d.	n.d.	n.d.	−17.3	−139
	39 [f]	6.6	2511	20	1818	8.7	26	262	30	317	49	1.4	53	326	1.2	n.d.	n.d.	n.d.	n.d.	112	n.d.	n.d.
15	25 [e]	6.4	2284	38	1647	19	20	263	26	270	39	1.1	42	484	n.d.	11	43	46	3.9	n.d.	n.d.	n.d.
	27 [f]	6.4	2265	51	1647	19	20	263	26	270	39	0.9	53	484	0.9	n.d.	n.d.	n.d.	n.d.	106	n.d.	n.d.
16	27 [e]	6.1	2151	−34	1540	19	23	208	26	293	42	3.2	41	915	0.9	n.d.	n.d.	n.d.	n.d.	n.d.	−17.8	−140
	30 [f]	6.5	2222	16	1598	25	20	244	25	277	40	1.6	41	408	1.0	n.d.	n.d.	n.d.	n.d.	90	n.d.	n.d.
17	22 [e]	6.1	1545	70	1085	45	14	190	24	163	24	0.1	26	1074	0.3	16	62	24	3.9	n.d.	−18.7	−142
	20 [f]	6.2	1908	156	1232	53	7.3	261	17.1	140	20	0.1	26	462	0.6	n.d.	n.d.	n.d.	n.d.	74	n.d.	n.d.
19	31 [e]	6.4	2140	142	1530	36	19	270	31	220	35	4.4	45	608	0.6	14	60	26	4.3	n.d.	−18.5	−142
	33 [f]	6.8	1928	142	1464	44	16	236	25	231	42	5.4	38	361	0.9	n.d.	n.d.	n.d.	n.d.	8.51	n.d.	n.d.
20 [f]	28 [f]	6.6	n.d.	142	n.d.	n.d.	n.d.	n.d.	n.d.	n.d.	n.d.	n.d.	n.d.	n.d.	n.d.	17	69	14	4.1	n.d.	n.d.	n.d.
22 [f]	27 [f]	6.3	n.d.	108	n.d.	n.d.	n.d.	n.d.	n.d.	n.d.	n.d.	n.d.	n.d.	n.d.	n.d.	9	41	50	4.6	4	n.d.	n.d.
31	27 [e]	6.4	2647	137	1910	21	28	288	37	319	45	0.1	43	736	0.4	n.d.	n.d.	n.d.	n.d.	n.d.	−18.8	−142
	27 [f]	6.5	1976	137	1757	8.8	16	262	28	280	41	0.3	46	380	0.9	n.d.	n.d.	n.d.	n.d.	58	n.d.	n.d.
32 [e]	27 [e]	6.5	2052	129	1464	23	23	190	31	282	39	n.d.	n.d.	565	0.2	17	70	13	4.2	65	−17.9	−139
									Lower temperature (T > 23 °C) thermal CO_2-rich waters													
2	18 [e]	6.2	1094	169	800	5.5	9.2	132	21	107	19	0.1	33	972	0.3	n.d.	n.d.	n.d.	n.d.	480	n.d.	n.d.
	21 [f]	6.1	1222	195	896	8.2	9.5	145	16	139	23	0.0	30	388	0.6	n.d.	n.d.	n.d.	n.d.	655	n.d.	n.d.
3	18 [e]	6.3	1235	190	906	5.3	8.9	154	23	117	20	0.01	33	760	0.1	11	43	46	3.9	n.d.	−16.0	−135
	21 [f]	6.2	1256	188	927	7.8	8.7	131	15	156	22	0	27	392	0.6	n.d.	n.d.	n.d.	n.d.	520	n.d.	n.d.

Table 1. *Cont.*

Loc. No	T (°C)	pH	TDS [a] (mg/L)	Eh (mV)	HCO_3^- (mg/L)	SO_4^{2-} (mg/L)	Cl^- (mg/L)	Ca^{2+} (mg/L)	Mg^{2+} (mg/L)	Na^+ (mg/L)	K^+ (mg/L)	Fe (mg/L)	SiO_2 (mg/L)	CO_2 [b] (mg/L)	F (mg/L)	O_2 (vol.%)	N_2 (vol.%)	CO_2 (vol.%)	N_2/O_2 (mol/mol)	^{222}Rn [c] (Bq/L)	$\delta^{18}O$ (%SMOW [d])	δ^2H (%SMOW [d])
							Lower temperature (T > 23 °C) thermal CO_2-rich waters															
4	12 [e]	5.9	607	188	450	4.5	5	82	17	41	7.4	0.1	21	1488	0.1	7	28	65	4.0	n.d.	−13.7	−127
	12 [f]	5.8	711	180	512	6.9	4.2	120	8.2	38	8.6	0.1	18	314	0.2	n.d.	n.d.	n.d.	n.d.	71	n.d.	n.d.
5	14 [e]	6.2	1018	200	744	4.8	11	108	22	111	18	0.2	28	946	0.3	14	56	30	4.0	n.d.	n.d.	n.d.
	17 [f]	6.0	1137	247	720	7.9	7.3	133	11	96	18	0.2	24	528	0.4	n.d.	n.d.	n.d.	n.d.	126	n.d.	n.d.
21a	13 [e]	6.2	1037	236	712	56	6.2	190	12	53	8.7	0.1	19	872	0.3	10	39	51	3.9	n.d.	n.d.	n.d.
	15 [f]	6.2	1426	224	824	63	3.6	225	13	63	10	0.1	18	370	0.4	n.d.	n.d.	n.d.	n.d.	51	n.d.	n.d.
23	16 [e]	6.5	1373	230	952	59	9.5	218	14	104	16	0.1	22	253	n.d.	14	55	31	3.9	n.d.	−18.2	−140
	17 [f]	6.7	1100	182	952	59	7.2	218	14	104	16	0.1	22	253	0.6	n.d.	n.d.	n.d.	n.d.	122	n.d.	n.d.
24	16 [e]	6.5	1158	188	800	51	9.5	181	18	85	15	0.1	22	553	0.5	15	60	25	4.0	n.d.	n.d.	n.d.
	17 [f]	6.6	1213	140	936	59	6.1	211	14	107	16	0	21	209	0.7	n.d.	n.d.	n.d.	n.d.	n.d.	n.d.	n.d.
25	16 [e]	6.4	1533	195	1110	11	18	220	18	136	20	n.d.	n.d.	600	0.2	10	51	39	5.1	n.d.	−17.3	−137
	16 [f]	6.7	1508	199	1098	58	14.8	255	20	108	25	0.3	25	352	0.5	n.d.	n.d.	n.d.	n.d.	93	n.d.	n.d.
26	20 [e]	6.2	1718	183	1220	31	19	220	24	178	26	0.1	33	1235	0.2	n.d.	n.d.	n.d.	n.d.	n.d.	−18.4	−140
	23 [f]	6.4	1737	217	1354	31	12.2	249	21	194	25	0.1	36	520	0.6	n.d.	n.d.	n.d.	n.d.	115	n.d.	n.d.
27	21 [e]	6.3	2064	169	1490	24	20	270	31	203	27	0.1	30	1252	0.3	7	32	61	4.6	400	n.d.	n.d.
	22 [f]	6.3	1611	240	1190	23	11.3	217	19	174	22	0.1	30	788	0.6	n.d.	n.d.	n.d.	n.d.	n.d.	n.d.	n.d.
28	13 [e]	6.3	1204	180	840	52	6.3	190	18	84	13	0.1	23	688	0.2	18	66	16	3.7	n.d.	n.d.	n.d.
	15 [f]	6.3	1520	216	1037	67	5.4	250	14	100	15	0.1	23	308	0.4	n.d.	n.d.	n.d.	n.d.	354	n.d.	n.d.
30	11 [e]	6.7	1546	228	1110	39	9.7	260	24	92	11	0.1	20	188	0.1	18	70	12	3.8	53	−17.9	−141
	13 [f]	6.8	1521	249	1001	44	6.8	227	16	106	15	0.1	22	228	0.3	n.d.	n.d.	n.d.	n.d.	53	n.d.	n.d.
							Shallow groundwaters															
29	12 [e]	7.8	289	169	200	15	4.4	56	7.3	3.0	3.4	0.1	1.1	41	0.1	n.d.	n.d.	n.d.	n.d.	n.d.	n.d.	n.d.
	13 [f]	7.8	294	249	213	2.6	0.3	76	0.8	0.4	0.5	0.2	1.0	5.5	< 0.1	n.d.	n.d.	n.d.	n.d.	62	n.d.	n.d.
29a [f]	14 [f]	6.6	n.d.	216	n.d.	n.d.	n.d.	n.d.	n.d.	n.d.	n.d.	n.d.	n.d.	n.d.	n.d.	16	65	19	4.1	62.	n.d.	n.d.
33	7.3 [e]	8.3	351	224	259	5.4	2.2	76	4.9	2.0	2.0	0.1	15	n.d.	0.1	19	75	6.0	3.9	n.d.	−16.8	−133
	n.d. [f]	8.3	453	224	319	23	0.5	98	7.7	2.2	2.4	0.1	18	4.4	< 0.1	n.d.	n.d.	n.d.	n.d.	n.d.	n.d.	n.d.

[a] Total Dissolved Solids; [b] volume of dissolved CO_2 per liter of water; [c] ^{222}Rn data from [26]; [d] Standard Mean Ocean Water; [e] data for samples collected in 2013 this study; [f] data for samples collected in 2011 from [26].

4.2. Dissolved Gas Composition

The gas composition of the studied springs is shown in Table 1and Figure 5 and reveals a relatively constant $N_2:O_2$ ratio (4.1 ± 1.0 mol/mol) just marginally higher than that of air (3.7) and with intermediate but highly variable proportions of CO_2. This suggests that the gases sampled are essentially mixtures of air and CO_2 with minor proportions of excess (i.e., above atmospheric composition) N_2. The CO_2 content of the analysedranged from 6 vol.% to 65 vol.%, with a broad overlap of compositions between Group I and Group II, but with the CO_2 contents of the shallow groundwaters (Group III) being distinctly lower than that of the thermal waters (Figures 5 and 6). Whilst relatively high oxygen contents are known to be characteristic of near surface waters [43], for the thermal waters, the variable oxygen (and highly correlated nitrogen) contents might reflect variable admixture of air during sampling of the springs at discharge. Highly variable gas CO_2 contents may also reflect this process and/or CO_2 exsolution/solution processes.
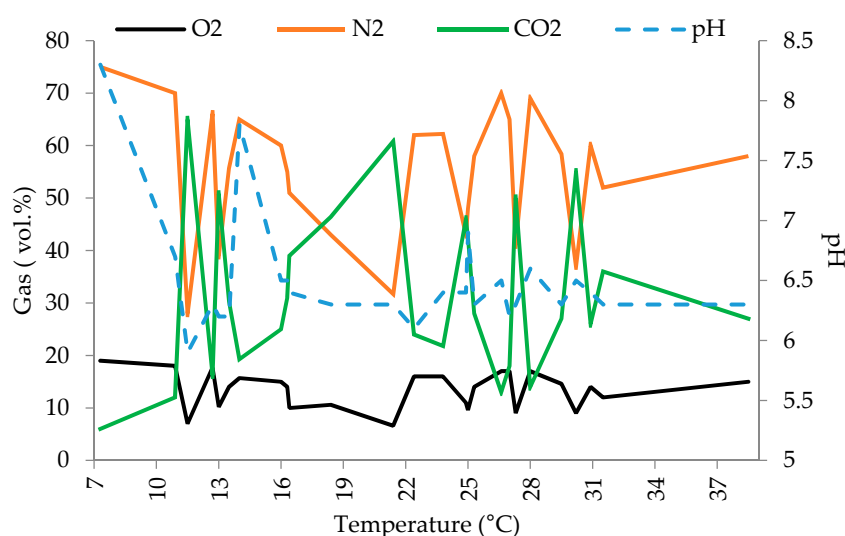

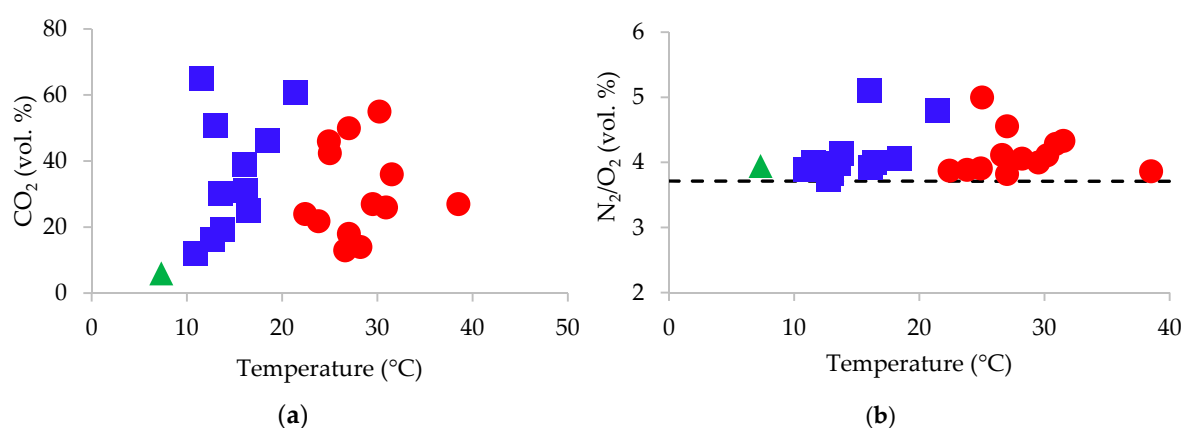**Figure 5.** Gas composition of groundwatersfrom the Choygan springs.

Figure 6. (**a**) CO_2 (vol.%) and (**b**) N_2/O_2 ratio in gas composition of the studied waters vs. temperature (°C). Symbols are the same as for Figure 3. Dashed line is the N_2/O_2 ratio in the air.

4.3. Radon-222 Concentration

The CO_2-rich Choygan waters contain appreciable radon (Table 1). However, the compositions of the higher temperature and lower temperature thermal CO_2-rich waters are broadly similar (4 Bq/L to

948 Bq/L cf. 53 Bq/L to 519 Bq/L) and, although elsewhere, higher radon concentrations are observed in waters with low mineralization [44]; in the Choygan waters, such a relationship is not apparent, there also being no significant relationship between radon and Na^+, Ca^{2+} and Mg^{2+}. The short half-life (3.82 days [45]) of radon-222, means that, in contrast to carbon dioxide, the source of radon is likely located near the springs, most probably from felsic rocks, enriched in uranium, and from which radon is produced by the alpha decay of radium-226, which is part of the radioactive uranium-238 series [44].

4.4. Geothermometers

Model reservoir temperatures, estimated using various geothermometers from the measured chemical compositions of the spring waters, are presented in Table 2. The lowest estimated reservoir temperatures are found using the chalcedony geothermometer, viz. 42–77 °C for the Group I (higher temperature thermal waters) and 31–52 °C forthe Group II (lower temperature thermal waters). The temperatures found by the quartz geothermometers are somewhat higher, viz. 74–107 °C for the higher temperature thermal water and 61–84 °C for the lower temperature thermal waters. The Na–K–Ca geothermometer gave rise to intermediate temperatures between the Na–K and silica geothermometers, viz. 84–119 °C and 42–84 °C, for the Group I and Group II thermal waters respectively. Significantly higher computed deep temperatures are obtained when using different Na–K geothermometers for low temperature thermal water as opposed to higher temperature thermal waters due to the high Ca^{2+} and Na^+ concentrations. The Na–K geothermometers give similar temperature values from 210 °C to 285 °C for both high and low temperature thermal CO_2-rich waters. Those temperatures are in disagreement with the values obtained with Na–K–Ca and silica geothermometers.

Mixing of thermal waters and colder groundwaters as well as a lack of a full chemical equilibrium may cause chemical geothermometers to provide uncertain results [3]. One of the requirements for the successful application of cation geothermometers is the attainment of water–rock equilibrium in the geothermal reservoir; the equilibrium can be evaluated by the Na–K–Mg triangular diagram [6]. The groundwater is evaluated with a Na–K–Mg ternary diagram proposed by Giggenbach (1988) [46] to identify the degree of maturation. According to the Na–K–Mg ternary diagram (Figure 7), all samples fall within the immature field, in particular, the Group III (shallow groundwaters) are very immature, consistent with unrealistically high model temperatures obtained by this approach, and both groups of thermal CO_2-rich waters are not in equilibrium, most likely because of being mixed with colder waters. Therefore, cation geothermometers do not likely yield realistic equilibration temperatures for these waters. The Na–K and Na–K–Ca geothermometers appear to provide unreliable estimations of the reservoir temperatures, which are too high (up to 285 °C). The quartz geothermometer is more suitable than cation geothermometers for such immature waters, giving lower and more reliable temperatures (63–107 °C) for the Choygan geothermal system.
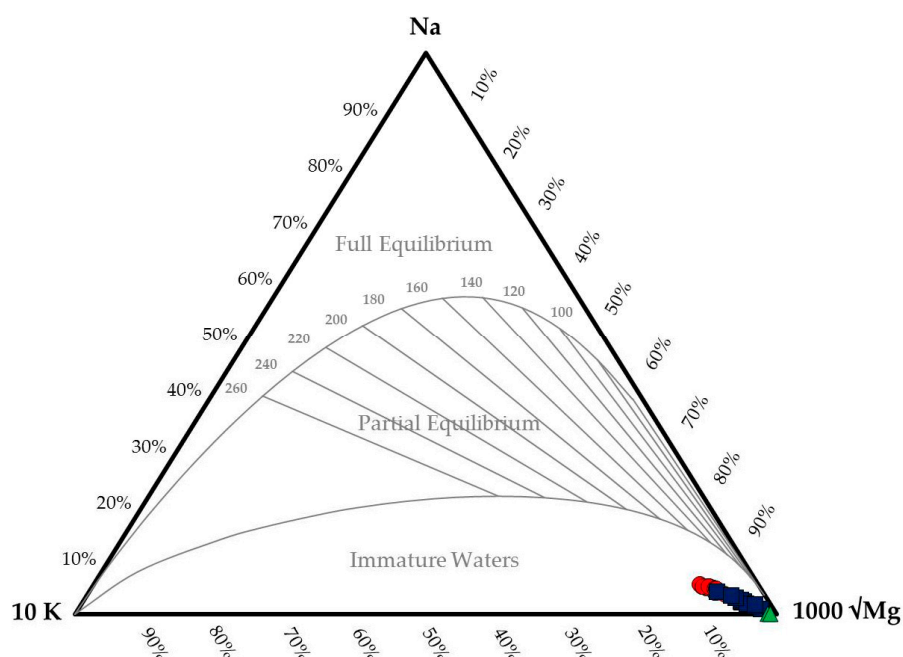
Figure 7. Giggenbach (Na–K–Mg$^{1/2}$) diagram [46] of the Choygan spring waters composition. Symbols are the same as for Figure 3.

Table 2. Geothermometry results for the Choygan spring waters (°C) (n.d. indicates no data).

Sample	Measured Spring Water	Chalcedony [a]	Quartz [b]	Na-K-Ca [c]	Na-K [d]	Na-K [e]	Na-K [f]
Group I (Higher temperature thermal CO$_2$-rich waters)							
1	22.6	72	103	117	233	262	237
6	29.5	72	103	114	250	276	254
7	23.8	65	96	115	252	277	255
8	25.3	71	101	100	230	260	234
9	27	67	97	112	257	281	260
9a	25	n.d.	n.d.	115	245	272	248
10	30.2	77	107	118	231	261	235
11	31.5	69	100	119	249	275	253
12	38.5	72	102	116	241	269	245
13	36.8	72	103	118	245	272	249
15	24.9	64	94	99	231	261	235
16	27	62	93	108	230	260	234
17	22.4	42	74	84	235	264	240
19	30.9	67	98	91	243	270	247
20	28.2	n.d.	n.d.	n.d.	n.d.	n.d.	n.d.
22	27.3	n.d.	n.d.	n.d.	n.d.	n.d.	n.d.
31	27.4	64	95	104	228	258	233
32	26.6	n.d.	n.d.	108	227	258	232
Group II (Lower temperature thermal CO$_2$-rich waters)							
2	17.5	52	83	79	262	285	264
3	18.4	52	84	79	255	280	258
4	11.5	34	66	51	260	283	262
5	13.5	45	77	82	244	271	248
21a	13	28	61	42	250	276	253
23	16.3	35	68	62	236	265	240
24	16.1	34	67	62	258	282	261
25	16.4	n.d.	n.d.	73	235	264	239
26	20.2	52	84	84	233	262	237
27	21.4	47	79	82	221	253	226
28	12.7	36	69	58	242	270	246
30	10.9	31	63	48	210	244	215

Table 2. *Cont.*

Sample	Measured Spring Water	Chalcedony [a]	Quartz [b]	Na-K-Ca [c]	Na-K [d]	Na-K [e]	Na-K [f]
Group III (Shallow groundwaters)							
29	12.3	n.d.	n.d.	250	842	629	760
29a	13.7	n.d.	n.d.	n.d.	n.d.	n.d.	n.d.
33	7.3	21	53	217	217	585	686

[a] Fournier (1977); [b] Fournier and Potter (1982); [c] Fournier and Truesdell (1973); [d] Truesdell (1976); [e] Fournier (1979); [f] Arnorsson et al. (1983b) [37].

4.5. Mineral Saturation States (SI)

As shown in Table 3, the waters of all the studied springs are oversaturated with respect to kaolinite, muscovite, k-feldspar and far from saturation with respect to anhydrite and gypsum at their discharge temperatures. However, in samples that have high SO_4 (>0.4 meq/L),the degree of undersaturation of sulfate minerals is lower and some springs are even in equilibrium with these minerals. The saturation indices of the silica minerals are above zero for both higher and lower temperature thermal CO_2-rich waters. Higher temperature thermal CO_2-rich waters are oversaturated or nearly in equilibrium with respect to the carbonate minerals and albite, while these minerals are unsaturated in the lower temperature thermal waters. The mineral saturation indices indicate the equilibrium state between higher temperature thermal waters and minerals such as calcite, aragonite and dolomite at the discharge temperatures and reflect a long residence time. Such behaviour is predictable due to the loss of CO_2 from the solution at atmospheric pressure, and, as a consequence, increases the solution pH, resulting in calcite precipitation in the discharge area. The shallow groundwater is undersaturated with respect to albite, kaolinite, muscovite, k-feldspar, silica and sulfate minerals and oversaturated with respect to carbonate minerals, reflecting the initial stage of water–rock interaction.

Table 3. Saturation indices, calculated at the measured discharge temperature, of selected minerals.

No	Albite	Muscovite	Kaolinite	K−Feldspar	Gypsum	Anhydrite	Calcite	Aragonite	Dolomite	Quartz	Chalcedony
				Group I (Higher temperature thermal CO_2-rich waters)							
1	−0.78	2.98	2.12	1.17	−2.91	−3.06	−0.13	−0.29	0.13	0.63	0.36
6	0.72	5.69	3.86	2.73	−2.76	−2.84	0.06	−0.10	0.61	0.92	0.65
7	0.90	6.14	4.13	2.91	−2.83	−2.96	0.00	−0.17	0.48	0.92	0.65
8	1.27	7.40	5.06	3.21	−3.04	−2.70	0.11	−0.05	0.35	0.91	0.64
9	0.66	5.86	4.05	2.69	−2.69	−2.80	−0.11	−0.28	0.19	0.91	0.64
9a	1.22	8.13	5.06	3.21	−2.86	−2.94	0.75	0.58	1.85	0.84	0.57
10	0.65	4.84	3.15	2.59	−2.69	−2.74	0.36	0.20	1.21	0.92	0.65
11	0.16	4.20	2.84	2.17	−2.73	−2.78	0.05	−0.12	0.43	0.88	0.60
12	0.59	5.13	3.46	2.57	−2.69	−2.68	0.13	−0.03	0.53	0.92	0.65
13	0.12	3.90	2.63	2.11	−2.77	−2.78	0.14	−0.03	0.62	0.89	0.62
15	0.86	6.33	4.28	2.81	−2.20	−2.30	0.27	0.11	0.71	0.86	0.58
16	1.18	9.83	6.75	3.11	−2.19	−2.35	0.00	−0.15	0.52	0.49	0.22
17	−0.46	4.40	3.33	1.50	−1.86	−1.97	−0.44	−0.60	−0.62	0.69	0.42
19	1.86	11.47	7.68	3.77	−1.83	−1.96	0.45	0.31	1.4	0.46	0.2
31	1.25	6.98	4.68	3.19	−2.17	−2.14	0.35	0.19	0.98	0.92	0.65
32	n.d.	n.d.	n.d.	n.d.	−2.22	n.d.	0.24	0.07	0.84	0.85	0.58
				Group II (Lower temperature thermal CO_2-rich waters)							
2	−1.00	2.74	2.22	1.04	−2.84	0.92	−3.02	−0.69	−0.70	0.73	0.46
3	−0.83	2.95	2.28	1.19	−2.83	−2.41	−3.00	−0.44	−0.22	0.73	0.46
4	0.96	7.99	6.19	2.99	−3.01	−4.92	−3.26	−1.58	−2.38	1.07	0.80
5	−0.27	6.33	4.63	1.72	−2.96	−2.69	−3.19	−0.80	−0.82	0.48	0.21
21a	−1.27	3.47	2.93	0.74	−1.72	−2.01	−1.92	−0.61	−0.94	0.57	0.30
23	−0.50	4.68	3.38	1.46	−1.69	**0.03**	−1.86	−0.09	0.13	0.55	0.28
24	−0.61	3.94	2.90	1.42	−1.80	**0.42**	−1.97	−0.15	0.16	0.66	0.39
25	n.d.	n.d.	n.d.	n.d.	−2.43	−1.24	0.07	−0.09	0.23	0.56	0.29
26	−0.76	4.23	3.14	1.18	−1.99	−1.20	−1.98	−0.33	−0.13	0.52	0.24
27	0.31	5.81	4.11	2.22	−2.07	−0.47	−2.06	−0.05	0.44	0.73	0.46
28	−0.64	4.90	3.70	1.34	−1.77	−1.11	−3.02	−0.39	−0.33	0.54	0.27
30	0.07	4.94	3.52	1.94	−1.86	2.18	−3.00	0.35	1.15	0.73	0.46
				Group III (Shallow groundwaters)							
29	−5.17	−0.22	−0.33	−2.29	−2.59	−2.79	0.52	0.36	1.30	−0.73	−1.00
33	−5.92	−3.08	−2.41	−3.12	−2.94	−3.18	1.24	1.08	2.44	−0.75	−1.02

Of course, thermal water compositions are more likely to reflect equilibrium between the waters and minerals (i.e., saturation) at deeper reservoir temperatures rather than at the discharge temperature. Thus, plotting SI with respect to several hydrothermal minerals as a function of temperature for several higher temperature thermal CO_2-rich springs (Figure 8) enables the intersection of the equilibrium lines for a group of selected minerals close to SI = 0 to be interpreted to reflect the most likely reservoir temperatures of those waters [3].
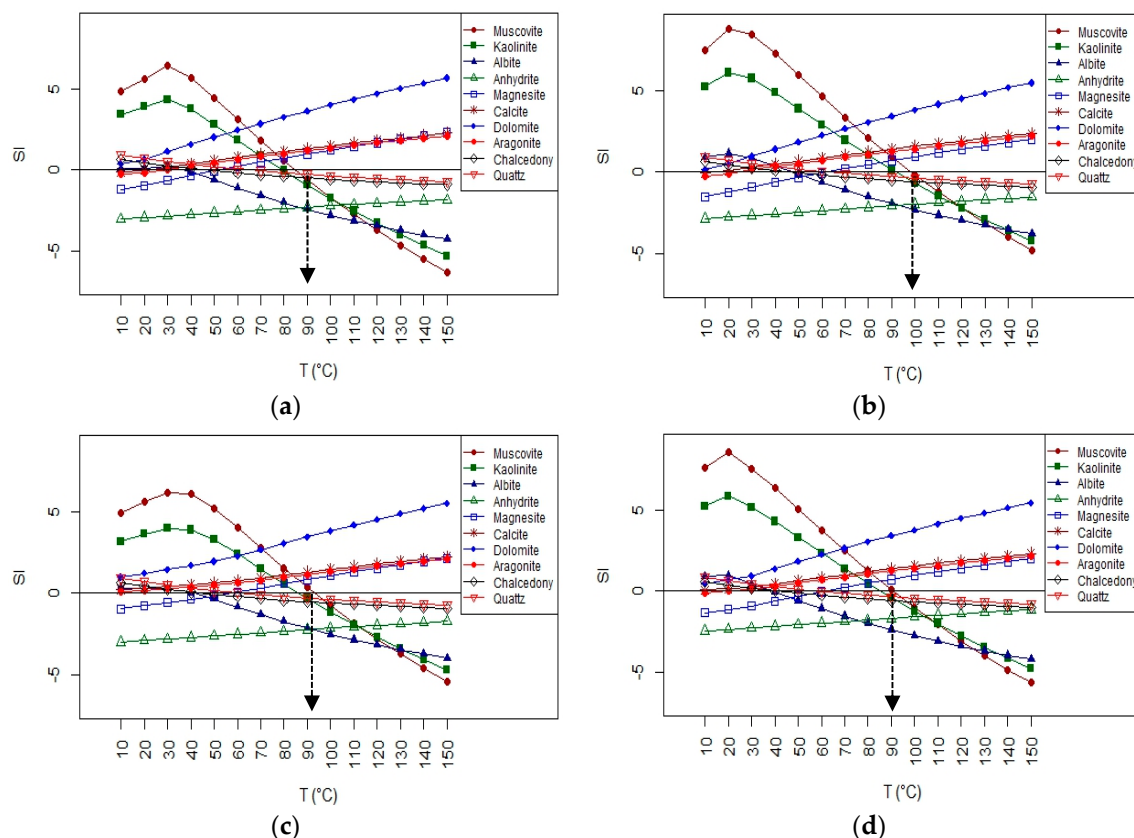

Figure 8. Changes in the saturation indices of selected minerals as a function of temperature: (**a**) Sample 6; (**b**) Sample 8; (**c**) Sample 12 and (**d**) Sample 15.

Whilst calcite, dolomite, aragonite, albite and quartz minerals are oversaturated or in equilibrium at the outflow conditions at 30–40 °C, which does not reflect the reservoir temperature, the SIs of muscovite, kaolinite, magnesite, chalcedony and quartz for the higher temperature thermal CO_2-rich waters converge and lie close to a SI = 0 at around 90–100 °C. This is the temperature at which the maximum number of mineral phases are in equilibrium with the waters and is thus interpreted as corresponding to the reservoir temperature. Anhydrite appears to be undersaturated at all temperatures and is of limited value in assessing likely reservoir temperatures. Calcite, aragonite, dolomite and magnesite are oversaturated at the modelled reservoir temperatures but closer to equilibrium at the observed discharge temperatures—this may reflect their involvement in lower temperature processes and/or the influence of changeable pCO_2—either way consideration of the temperature dependence of their SIs does not provide a reliable estimate of reservoir temperature.

The aqueous activities of $Ca^{++}(aq)$, $Mg^{++}(aq)$, $Na^+(aq)$, $K^+(aq)$, and $H^+(aq)$ for the Choygan springs are plotted in $M^{z+}(aq)/aH^+(aq)^z$ vs. SiO_2 activity–activity diagrams at temperatures of 25 °C, 100 °C, and 170 °C, bracketing the likely ranges of reservoir and near surface temperatures of the thermal waters and groundwaters (Figure 9).
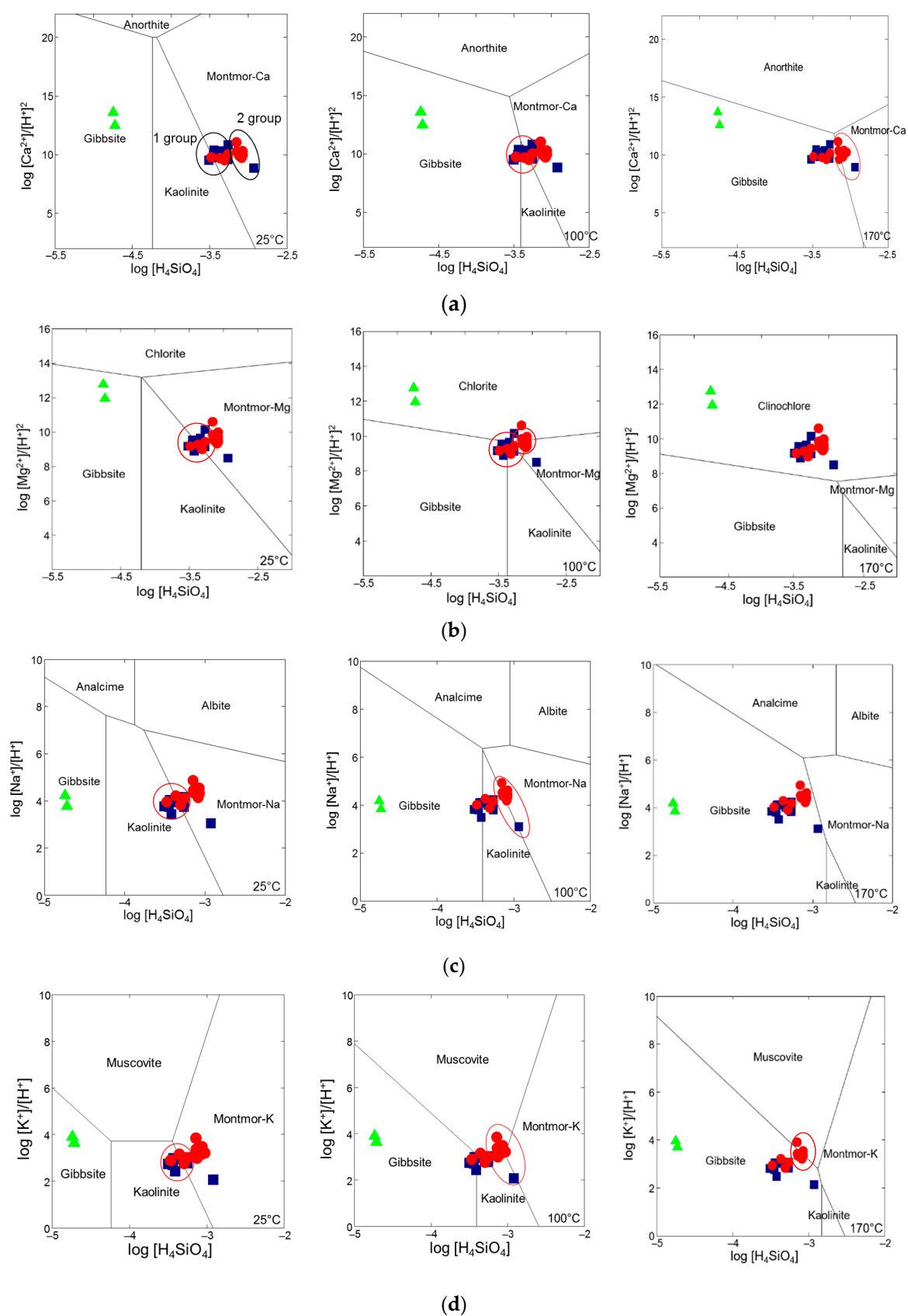
Figure 9. $[M^{z+}]/[H^+]^z – [H_4SiO_4]$ activity-activity diagrams at 25 °C, 100 °C, and 170 °C for (**a**) Ca; (**b**) Mg; (**c**) Na; (**d**) K. Symbols are as for Figure 3.

Two groups are clearly distinguishable: Group 1 includes nine lower temperature and four higher temperature thermal CO_2-rich springs and Group 2 consisting of 14 higher temperature and one lower temperature thermal CO_2-rich springs. Interestingly, the springs of Group 1 are located on the periphery of the study area, whereas the springs of Group 2 are found in the central part of the study area.

Group 1 waters fall into the kaolinite stability field at 25 °C, but more closely reflect the coexistence of gibbsite, kaolinite, muscovite and Ca-, Mg-, K-montmorillonite phases at 100 °C. Similarly, Group 2 water compositions most closely reflect coexistence of multiple silicate phases at 100 °C (cf. 25 °C or 170 °C) consistent with saturation states calculated from the chemical geothermometers. Thus, to a large exent, the mineral assemblage kaolinite-muscovite-Ca-, Mg-, Na-, and K-montmorillonite influences the chemical composition of both the higher and lower temperature thermal CO_2-rich waters, whilst 100°C appears to be a highly plausible best reservoir temperature of the Choygan geothermal system.

In addition to temperature, the partial pressure of CO_2 affects the precipitation and dissolution of different minerals. The solubility of CO_2 in water decreases with increasing temperature and salinity but increases with pressure [47]. Calculations of saturation indices were therefore performed at the inferred reservoir temperature (95 °C) and at different CO_2 pressures to demonstrate the influence of pCO_2 (Figure 10), viz. as pCO_2 increases the pH values and carbonate and iron mineral saturation indices states rapidly decrease, but the SI values of the silicate minerals are largely unaffected.
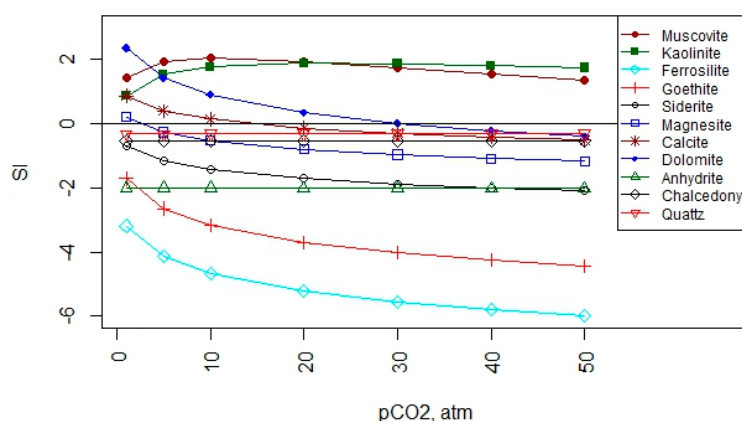

Figure 10. Saturation indices of the selected minerals as a function of partial pressure of CO_2 (Group I higher temperature thermal CO_2-rich water: Sample 8).

The multicomponent geothermometry approach for temperature estimations included statistical analyses of saturation indices the following minerals: muscovite, kaolinite, montmorillonite (Ca, Na, K, Mg), quartz, and chalcedony. These minerals were chosen as a potential mineral assemblage of Choygan geothermal system following on results of the saturation indices and equilibrium states and controlling of chemistry of water samples. The results of statistical analyses of saturation indices are shown in Table 4.

The computed mineral saturation indices (log(Q/K)) as a function of temperature indicate reservoir temperatures largely ranging from 40 °C (in Group II) to 80 °C (in Group I) with no convergence established for the shallow groundwater samples and significantly higher temperatures, 130 °C and 180 °C, determined for samples 16 and 19, respectively (Figure 11; Table 4).

Summarizing the saturation states of the selected minerals (Figures 8 and 9) and the statistical analysis of the saturation indices (Figure 11), the reservoir temperature is estimated to be between 70 °C and 100 °C for the Choygan geothermal system. This is consistent with the quartz geothermometer derived reservoir temperature of 98 °C.

This estimated reservoir temperature at a depth of 3 km is consistent with the area's high heat flow (84 MW/m^2) and geothermal gradient (33.6 °C/km) [32], determined elsewhere by an isotope helium assessment in the Eastern Tuva territory [32]. Compared to the Eastern Tuva, in the Western Tuva, the average heat flow is much lower, ~45–50 mW/m^2.

Figure 11. Statistical analyses of saturation indices: median, mean standard deviation (SDEV) and mean root square error (RMSE) of absolute log(Q/K) values as a function of model reservoir temperature (Group I higher temperature thermal CO$_2$-rich water: Sample 8). The reservoir temperature is inferred from the temperature at which the value of the median is a minimum. Group I higher temperature thermal CO$_2$-rich springs: (**a**) Sample 6; (**b**) Sample 12; Group II lower temperature thermal CO$_2$-rich springs: (**c**) Sample 28; (**d**) Sample 2; (**e**) Sample 4; Group III shallow groundwater: (**f**) Sample 29.
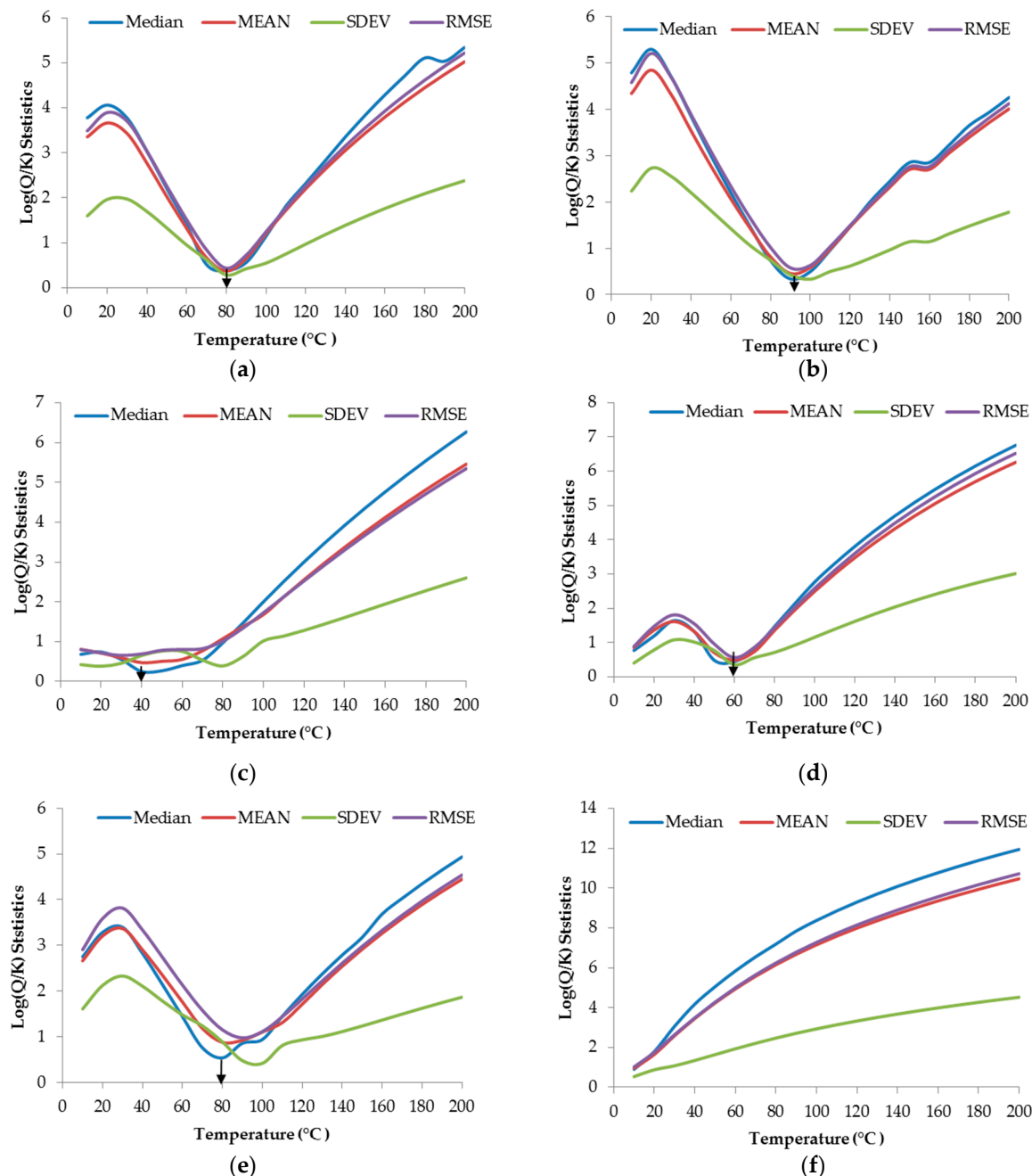
Table 4. Statistical analyses of saturation indices: median, mean standard deviation (SDEV) and mean root square error (RMSE) of absolute log(Q/K) vs. temperature. The estimated temperatures are given by the minimum median of absolute log(Q/K) values.

No	Statistical Parameter	Temperature (°C)																			
		10	20	30	40	50	60	70	80	90	100	110	120	130	140	150	160	170	180	190	200
		Group I (Higher temperature thermal CO_2-rich waters)																			
1	Median	2.49	2.50	2.56	2.17	1.50	0.62	**0.29** [a]	0.57	1.20	1.90	2.47	3.05	3.72	4.37	5.00	5.45	5.89	6.30	6.70	7.09
	MEAN	2.25	2.35	2.35	2.02	1.43	0.78	0.37	0.59	1.18	1.76	2.30	2.82	3.31	3.78	4.23	4.65	5.06	5.45	5.83	6.20
	SDEV	0.93	1.16	1.32	1.26	1.01	0.70	0.35	0.44	0.59	0.82	1.07	1.33	1.58	1.82	2.06	2.29	2.51	2.73	2.93	3.13
	RMSE	2.29	2.46	2.52	2.23	1.63	0.97	0.47	0.68	1.24	1.82	2.39	2.93	3.45	3.94	4.41	4.87	5.30	5.72	6.12	6.51
6	Median	3.78	4.06	3.78	3.04	2.21	1.41	0.52	**0.38**	0.56	1.15	1.81	2.32	2.83	3.35	3.84	4.29	4.71	5.11	5.04	5.34
	MEAN	3.36	3.66	3.43	2.77	2.03	1.32	0.67	0.37	0.65	1.21	1.72	2.20	2.64	3.06	3.44	3.80	4.13	4.45	4.74	5.02
	SDEV	1.60	1.96	1.97	1.70	1.33	0.95	0.63	0.29	0.42	0.55	0.75	0.97	1.18	1.39	1.58	1.76	1.93	2.09	2.24	2.38
	RMSE	3.49	3.89	3.70	3.04	2.26	1.52	0.85	0.43	0.72	1.25	1.77	2.26	2.72	3.15	3.56	3.93	4.29	4.62	4.93	5.22
7	Median	4.72	4.78	4.15	3.29	2.43	1.61	0.85	**0.26** [a]	0.52	0.97	1.51	2.14	2.61	3.05	3.51	3.96	4.38	4.78	4.85	5.16
	MEAN	4.27	4.38	3.82	3.05	2.28	1.56	0.92	0.44	0.56	1.00	1.52	2.00	2.44	2.85	3.24	3.60	3.93	4.24	4.54	4.82
	SDEV	2.23	2.48	2.28	1.93	1.52	1.14	0.78	0.46	0.32	0.49	0.64	0.83	1.03	1.23	1.41	1.59	1.76	1.92	2.07	2.20
	RMSE	4.52	4.71	4.16	3.37	2.56	1.80	1.11	0.59	0.60	1.05	1.55	2.03	2.49	2.92	3.32	3.70	4.05	4.38	4.69	4.98
8	Median	4.79	5.29	4.70	3.85	3.00	2.20	1.45	0.73	**0.34** [a]	0.50	0.96	1.46	2.00	2.44	2.85	2.85	3.23	3.65	3.93	4.25
	MEAN	4.34	4.84	4.31	3.53	2.77	2.06	1.41	0.81	0.46	0.59	0.98	1.46	1.91	2.32	2.70	2.70	3.06	3.40	3.71	4.01
	SDEV	2.23	2.73	2.55	2.20	1.81	1.42	1.05	0.74	0.43	0.33	0.50	0.62	0.78	0.96	1.14	1.14	1.32	1.48	1.63	1.78
	RMSE	4.58	5.20	4.69	3.88	3.09	2.34	1.64	1.02	0.58	0.63	1.04	1.49	1.94	2.36	2.76	2.76	3.13	3.48	3.81	4.12
9	Median	2.60	3.14	3.36	3.02	2.31	1.52	0.77	**0.30** [a]	0.52	0.76	1.18	1.83	2.40	2.83	3.24	3.63	4.02	4.39	4.62	4.93
	MEAN	2.33	2.77	2.99	2.72	2.15	1.52	0.96	0.52	0.55	0.82	1.29	1.74	2.15	2.53	2.89	3.23	3.54	3.83	4.11	4.37
	SDEV	1.11	1.64	1.99	1.96	1.64	1.27	0.88	0.55	0.24	0.49	0.59	0.77	0.96	1.16	1.35	1.53	1.70	1.86	2.01	2.15
	RMSE	2.56	3.17	3.53	3.29	2.65	1.94	1.27	0.74	0.60	0.94	1.41	1.88	2.34	2.76	3.16	3.54	3.89	4.22	4.53	4.82
9a	Median	5.52	5.15	4.19	3.23	2.33	1.49	0.68	**0.30** [a]	0.59	1.26	1.95	2.69	3.36	3.97	4.44	4.90	5.33	5.75	6.14	6.53
	MEAN	4.93	4.65	3.80	2.94	2.15	1.41	0.75	0.38	0.68	1.26	1.81	2.34	2.83	3.30	3.75	4.17	4.58	4.97	5.34	5.70
	SDEV	2.63	2.63	2.25	1.86	1.43	1.03	0.67	0.34	0.38	0.52	0.74	0.99	1.24	1.48	1.72	1.95	2.16	2.37	2.57	2.77
	RMSE	5.24	4.99	4.13	3.24	2.40	1.62	0.93	0.47	0.73	1.28	1.84	2.39	2.91	3.40	3.87	4.32	4.75	5.17	5.56	5.95
10	Median	0.84	0.76	0.43	0.31	0.24	0.41	**0.29** [a]	0.35	0.51	1.06	1.59	2.23	2.72	3.19	3.63	4.23	4.81	5.38	5.86	6.24
	MEAN	1.12	0.85	0.50	0.34	0.43	0.68	0.57	0.46	0.63	1.01	1.53	2.02	2.50	2.95	3.39	3.81	4.21	4.60	4.98	5.35
	SDEV	0.62	0.47	0.35	0.26	0.56	0.72	0.71	0.42	0.35	0.59	0.73	0.92	1.14	1.36	1.58	1.80	2.01	2.22	2.42	2.62
	RMSE	1.20	0.90	0.57	0.40	0.65	0.91	0.83	0.57	0.67	1.10	1.59	2.09	2.58	3.05	3.51	3.96	4.38	4.80	5.20	5.59
11	Median	2.31	2.12	1.87	1.51	1.02	0.58	**0.32** [a]	**0.32** [a]	0.51	0.72	1.06	1.54	2.01	2.45	3.01	3.43	3.83	4.22	4.70	5.23
	MEAN	2.39	2.11	1.74	1.30	0.83	0.60	0.52	0.59	0.62	0.77	0.92	1.37	1.83	2.27	2.70	3.11	3.51	3.89	4.27	4.63
	SDEV	1.23	1.10	0.95	0.80	0.64	0.32	0.57	0.71	0.54	0.27	0.64	0.72	0.83	0.98	1.16	1.34	1.54	1.73	1.92	2.11
	RMSE	2.52	2.23	1.86	1.43	0.97	0.64	0.71	0.85	0.76	0.77	1.05	1.45	1.88	2.33	2.76	3.19	3.60	4.00	4.40	4.78

Table 4. *Cont.*

No	Statistical Parameter	Temperature (°C)																			
		10	20	30	40	50	60	70	80	90	100	110	120	130	140	150	160	170	180	190	200
		Group I (Higher temperature thermal CO_2-rich waters)																			
12	Median	2.48	3.06	3.30	2.93	2.19	1.40	0.56	**0.39** [a]	0.61	1.19	1.77	2.33	2.80	3.29	3.78	4.23	4.65	5.05	5.06	5.37
	MEAN	2.24	2.76	3.02	2.70	2.04	1.34	0.69	0.38	0.65	1.19	1.70	2.18	2.63	3.04	3.42	3.78	4.12	4.44	4.73	5.01
	SDEV	0.93	1.42	1.74	1.67	1.36	0.99	0.67	0.33	0.42	0.55	0.74	0.96	1.17	1.37	1.56	1.74	1.91	2.07	2.22	2.36
	RMSE	2.29	2.91	3.26	2.97	2.28	1.55	0.89	0.47	0.72	1.23	1.75	2.24	2.70	3.13	3.54	3.91	4.27	4.60	4.91	5.20
13	Median	2.04	1.84	1.59	1.23	0.74	0.61	**0.21** [a]	0.30	0.46	0.65	0.93	1.41	1.88	2.33	2.88	3.30	3.71	4.10	4.65	5.19
	MEAN	2.17	1.89	1.53	1.09	0.66	0.51	0.52	0.64	0.56	0.71	0.86	1.27	1.73	2.18	2.61	3.02	3.42	3.80	4.18	4.54
	SDEV	1.11	0.97	0.82	0.68	0.50	0.33	0.69	0.77	0.62	0.27	0.56	0.68	0.78	0.94	1.12	1.31	1.50	1.69	1.89	2.08
	RMSE	2.29	1.99	1.62	1.19	0.77	0.57	0.79	0.92	0.77	0.71	0.96	1.35	1.79	2.23	2.67	3.09	3.51	3.91	4.31	4.69
15	Median	3.45	3.32	2.98	2.54	2.01	1.43	0.84	**0.31** [a]	0.56	0.81	1.33	1.82	2.30	2.84	3.28	3.70	4.11	4.50	4.99	5.52
	MEAN	3.26	3.19	2.91	2.53	2.09	1.59	1.10	0.70	0.68	0.86	1.14	1.62	2.09	2.54	2.97	3.39	3.79	4.17	4.54	4.91
	SDEV	1.68	1.84	1.84	1.75	1.56	1.33	1.08	0.81	0.42	0.39	0.71	0.79	0.92	1.09	1.28	1.48	1.67	1.87	2.06	2.25
	RMSE	3.44	3.45	3.21	2.87	2.42	1.92	1.42	0.98	0.75	0.88	1.25	1.69	2.15	2.60	3.04	3.47	3.89	4.30	4.69	5.07
16	Median	4.28	4.85	5.40	5.55	5.05	4.42	3.74	3.07	2.44	1.86	1.32	0.81	**0.66** [a]	0.73	0.79	0.85	1.12	1.45	1.73	2.33
	MEAN	3.97	4.53	5.08	5.24	4.82	4.29	3.70	3.13	2.58	2.08	1.60	1.16	0.87	0.71	0.80	0.92	1.12	1.39	1.69	1.97
	SDEV	2.10	2.64	3.14	3.38	3.17	2.86	2.48	2.11	1.77	1.48	1.24	1.05	0.80	0.62	0.39	0.46	0.61	0.67	0.69	0.74
	RMSE	4.21	4.91	5.57	5.81	5.38	4.80	4.15	3.52	2.92	2.37	1.88	1.45	1.10	0.88	0.84	0.97	1.19	1.45	1.72	1.98
17	Median	2.46	2.32	2.07	1.71	1.29	0.93	**0.75** [a]	0.92	1.26	1.73	2.20	2.66	3.11	3.54	4.05	4.46	4.85	5.23	5.60	5.95
	MEAN	2.27	2.00	1.65	1.28	1.01	0.95	0.95	1.04	1.18	1.37	1.76	2.21	2.65	3.08	3.49	3.89	4.28	4.66	5.02	5.37
	SDEV	1.23	1.18	1.10	0.95	0.71	0.40	0.43	0.37	0.51	0.88	1.03	1.11	1.22	1.37	1.53	1.69	1.87	2.04	2.22	2.39
	RMSE	2.42	2.17	1.84	1.48	1.15	0.97	0.98	1.04	1.21	1.52	1.90	2.32	2.74	3.17	3.58	3.99	4.39	4.78	5.16	5.53
19	Median	5.20	5.64	6.11	6.59	6.70	5.94	5.21	4.52	3.87	3.26	2.69	2.15	1.65	1.17	0.81	0.56	0.80	**0.67** [a]	1.02	1.28
	MEAN	4.68	5.14	5.61	6.09	6.24	5.57	4.95	4.35	3.78	3.24	2.73	2.24	1.78	1.34	0.95	0.73	0.60	0.81	1.04	1.39
	SDEV	2.46	2.93	3.39	3.84	4.00	3.62	3.21	2.81	2.44	2.09	1.76	1.47	1.21	1.00	0.82	0.56	0.51	0.36	0.51	0.48
	RMSE	4.96	5.53	6.13	6.72	6.92	6.20	5.50	4.83	4.20	3.60	3.03	2.50	2.00	1.55	1.16	0.85	0.73	0.83	1.08	1.39
21a	Median	2.55	2.43	2.18	1.84	1.44	1.19	**1.10** [a]	1.39	1.86	2.36	2.86	3.34	3.80	4.24	4.67	5.08	5.47	5.85	6.22	6.58
	MEAN	2.13	1.91	1.66	1.46	1.30	1.17	1.19	1.38	1.66	1.94	2.37	2.79	3.20	3.59	3.97	4.34	4.69	5.03	5.35	5.67
	SDEV	1.33	1.36	1.27	1.02	0.68	0.49	0.46	0.53	0.81	1.18	1.30	1.44	1.58	1.74	1.90	2.06	2.22	2.38	2.54	2.70
	RMSE	2.20	2.05	1.83	1.56	1.30	1.13	1.13	1.32	1.63	2.00	2.38	2.77	3.15	3.53	3.89	4.25	4.59	4.92	5.24	5.55
31	Median	0.44	0.39	0.43	0.78	1.12	1.21	0.92	0.54	**0.36** [a]	0.60	0.98	1.48	1.96	2.41	2.85	3.28	3.68	4.10	4.56	5.01
	MEAN	0.47	0.47	0.59	0.85	1.12	1.22	1.04	0.66	0.46	0.68	0.98	1.37	1.79	2.19	2.58	2.96	3.32	3.66	4.00	4.33
	SDEV	0.28	0.32	0.49	0.68	0.85	0.94	0.83	0.68	0.48	0.27	0.50	0.69	0.83	0.99	1.16	1.34	1.52	1.70	1.87	2.04
	RMSE	0.48	0.50	0.67	0.94	1.23	1.35	1.16	0.82	0.57	0.65	0.97	1.35	1.74	2.13	2.51	2.87	3.23	3.57	3.91	4.23

Table 4. *Cont.*

No	Statistical Parameter	Temperature (°C)																		
		10	20	30	40	50	60	70	80	90	100	110	120	130	140	150	160	170	180	190	200
		Group II (Lower temperature thermal CO$_2$-rich waters)																			
2	Median	0.77	1.19	1.65	1.33	0.48	**0.45** [a]	0.80	1.47	2.13	2.77	3.31	3.81	4.27	4.70	5.10	5.47	5.82	6.15	6.46	6.75
	MEAN	3.04	3.12	2.90	2.43	1.91	1.42	1.01	0.84	1.00	1.32	1.72	2.10	2.46	2.79	3.10	3.39	3.67	3.92	4.17	4.40
	SDEV	2.69	2.59	2.36	1.96	1.56	1.20	0.98	0.83	0.75	0.79	0.80	0.92	1.09	1.29	1.49	1.69	1.88	2.07	2.25	2.42
	RMSE	4.01	4.00	3.69	3.08	2.43	1.84	1.39	1.16	1.24	1.52	1.89	2.28	2.68	3.06	3.42	3.76	4.09	4.40	4.70	4.98
3	Median	2.76	2.57	1.96	1.06	**0.24** [a]	0.47	1.11	1.80	2.52	3.13	3.69	4.23	4.76	5.40	6.03	6.62	7.20	7.63	8.01	8.38
	MEAN	2.58	2.35	1.83	1.14	0.48	0.56	1.02	1.67	2.28	2.86	3.41	3.92	4.41	4.88	5.32	5.74	6.14	6.52	6.89	7.24
	SDEV	1.28	1.33	1.18	0.90	0.61	0.29	0.62	0.83	1.08	1.35	1.62	1.88	2.13	2.38	2.61	2.84	3.05	3.26	3.46	3.65
	RMSE	2.70	2.53	2.03	1.35	0.71	0.59	1.12	1.75	2.37	2.97	3.54	4.08	4.60	5.09	5.56	6.01	6.43	6.84	7.23	7.60
4	Median	2.75	3.29	3.40	2.82	2.14	1.44	0.76	**0.54** [a]	0.86	0.94	1.45	1.93	2.38	2.79	3.17	3.69	4.03	4.35	4.49	4.94
	MEAN	2.66	3.21	3.37	2.90	2.34	1.76	1.18	0.88	0.93	1.11	1.31	1.71	2.14	2.54	2.92	3.27	3.59	3.89	4.18	4.45
	SDEV	1.61	2.13	2.33	2.11	1.78	1.48	1.24	0.89	0.48	0.42	0.81	0.93	1.01	1.11	1.24	1.37	1.50	1.63	1.75	1.87
	RMSE	4.01	4.00	3.69	3.08	2.43	1.84	1.39	1.16	1.24	1.52	1.89	2.28	2.68	3.06	3.42	3.76	4.09	4.40	4.70	4.98
5	Median	2.93	2.99	3.04	2.90	2.47	1.84	1.18	0.63	**0.62** [a]	0.82	1.10	1.62	2.10	2.56	3.15	3.57	3.97	4.36	4.74	5.27
	MEAN	2.76	2.88	2.97	2.91	2.58	2.06	1.50	0.96	0.72	0.88	1.04	1.48	1.96	2.42	2.86	3.28	3.68	4.06	4.43	4.78
	SDEV	1.51	1.78	2.01	2.04	1.88	1.58	1.29	1.04	0.70	0.29	0.64	0.75	0.83	0.97	1.14	1.32	1.51	1.70	1.88	2.07
	RMSE	2.95	3.16	3.35	3.31	2.96	2.42	1.83	1.30	0.93	0.87	1.15	1.56	2.01	2.46	2.90	3.33	3.74	4.14	4.53	4.90
23	Median	2.60	2.98	3.32	2.84	2.21	1.56	0.92	**0.57** [a]	0.62	0.81	1.07	1.63	2.11	2.58	3.02	3.44	3.85	4.24	4.62	4.98
	MEAN	2.35	2.69	3.02	2.67	2.23	1.75	1.27	0.83	0.69	0.91	1.21	1.49	1.86	2.27	2.66	3.04	3.40	3.74	4.08	4.40
	SDEV	1.33	1.72	2.01	1.85	1.56	1.29	1.08	0.93	0.71	0.43	0.42	0.75	0.93	1.04	1.17	1.32	1.47	1.63	1.78	1.94
	RMSE	2.38	2.81	3.18	2.84	2.38	1.91	1.45	1.07	0.85	0.89	1.13	1.47	1.84	2.21	2.57	2.93	3.28	3.61	3.94	4.26
24	Median	1.82	1.69	1.45	1.13	0.96	**0.84** [a]	1.11	1.64	2.22	2.77	3.31	3.81	4.30	4.76	5.20	5.62	6.03	6.42	6.79	7.16
	MEAN	1.61	1.40	1.14	1.00	0.89	0.90	1.11	1.43	1.84	2.33	2.80	3.24	3.67	4.08	4.47	4.84	5.20	5.55	5.88	6.20
	SDEV	0.95	0.97	0.90	0.63	0.42	0.38	0.45	0.79	1.06	1.22	1.40	1.59	1.78	1.97	2.16	2.34	2.52	2.70	2.87	3.04
	RMSE	1.65	1.49	1.27	1.03	0.87	0.86	1.07	1.43	1.87	2.32	2.76	3.19	3.60	4.00	4.39	4.75	5.11	5.45	5.78	6.10
26	Median	0.75	0.60	0.52	0.29	**0.24** [a]	0.36	0.27	0.46	0.86	1.27	1.76	2.24	2.70	3.14	3.56	3.97	4.36	4.74	5.11	5.47
	MEAN	0.84	0.74	0.59	0.43	0.43	0.54	0.53	0.65	0.94	1.22	1.53	1.95	2.36	2.75	3.13	3.49	3.84	4.18	4.51	4.83
	SDEV	0.55	0.40	0.37	0.54	0.72	0.78	0.70	0.51	0.35	0.58	0.90	1.02	1.16	1.32	1.48	1.65	1.81	1.98	2.14	2.30
	RMSE	0.88	0.74	0.61	0.59	0.71	0.81	0.76	0.72	0.89	1.20	1.56	1.94	2.32	2.69	3.06	3.41	3.76	4.09	4.41	4.73
27	Median	3.44	3.41	3.19	2.62	1.87	1.10	**0.41** [a]	0.62	0.91	1.51	2.07	2.65	3.19	3.67	4.12	4.61	5.19	5.74	6.28	6.80
	MEAN	3.16	3.19	3.02	2.55	1.92	1.27	0.71	0.65	0.86	1.37	1.91	2.43	2.92	3.38	3.83	4.25	4.65	5.04	5.41	5.76
	SDEV	1.70	1.91	1.97	1.76	1.43	1.08	0.78	0.34	0.53	0.67	0.81	1.01	1.22	1.44	1.66	1.88	2.09	2.29	2.49	2.67
	RMSE	3.36	3.48	3.37	2.89	2.22	1.55	0.97	0.69	0.94	1.43	1.95	2.47	2.98	3.46	3.92	4.37	4.79	5.20	5.59	5.97

Table 4. *Cont.*

No	Statistical Parameter	Temperature (°C)																			
		10	20	30	40	50	60	70	80	90	100	110	120	130	140	150	160	170	180	190	200
		Group II (Lower temperature thermal CO_2-rich waters)																			
28	Median	0.68	0.74	0.55	**0.25** [a]	0.27	0.40	0.53	0.97	1.47	2.00	2.51	3.00	3.47	3.92	4.35	4.76	5.16	5.54	5.91	6.27
	MEAN	0.80	0.72	0.60	0.47	0.51	0.55	0.77	1.08	1.38	1.68	2.13	2.56	2.97	3.37	3.75	4.12	4.47	4.81	5.14	5.46
	SDEV	0.42	0.38	0.46	0.66	0.76	0.76	0.54	0.39	0.63	1.02	1.14	1.28	1.44	1.61	1.78	1.95	2.11	2.28	2.44	2.60
	RMSE	0.80	0.72	0.66	0.69	0.78	0.80	0.82	1.02	1.34	1.73	2.13	2.53	2.92	3.30	3.67	4.03	4.38	4.71	5.03	5.35
30	Median	2.23	2.09	1.79	1.24	0.62	**0.39** [a]	0.69	1.24	1.86	2.44	3.00	3.52	4.01	4.48	4.92	5.34	5.75	6.13	6.51	6.95
	MEAN	2.00	1.91	1.70	1.31	0.82	0.54	0.85	1.22	1.62	2.13	2.61	3.07	3.50	3.91	4.31	4.68	5.04	5.38	5.71	6.03
	SDEV	1.12	1.25	1.22	1.05	0.85	0.64	0.34	0.56	0.92	1.07	1.26	1.45	1.64	1.84	2.03	2.22	2.40	2.57	2.74	2.91
	RMSE	2.02	2.00	1.83	1.47	1.02	0.72	0.81	1.19	1.64	2.10	2.56	3.00	3.42	3.82	4.21	4.58	4.93	5.27	5.60	5.92
		Shallow groundwaters																			
29	Median	**0.90** [a]	1.79	3.07	4.18	5.05	5.84	6.55	7.19	7.85	8.37	8.86	9.30	9.70	10.08	10.44	10.77	11.09	11.39	11.67	11.94
	MEAN	0.95	1.65	2.59	3.45	4.23	4.94	5.58	6.15	6.68	7.15	7.59	7.99	8.37	8.71	9.04	9.36	9.65	9.94	10.21	10.47
	SDEV	0.54	0.88	1.08	1.35	1.64	1.93	2.21	2.47	2.71	2.93	3.14	3.33	3.51	3.68	3.83	3.98	4.13	4.26	4.39	4.52
	RMSE	1.02	1.75	2.64	3.49	4.28	4.99	5.65	6.24	6.78	7.27	7.73	8.15	8.53	8.90	9.24	9.57	9.87	10.17	10.45	10.72
33	Median	**1.17** [a]	2.16	3.04	3.82	4.52	5.14	5.69	6.19	6.62	7.02	7.37	7.70	7.99	8.26	8.52	8.75	8.97	9.19	9.39	9.58
	MEAN	1.32	2.10	2.79	3.41	3.95	4.44	4.87	5.26	5.61	5.92	6.21	6.47	6.71	6.93	7.13	7.33	7.51	7.69	7.85	8.02
	SDEV	0.84	1.10	1.39	1.67	1.93	2.17	2.38	2.58	2.76	2.93	3.07	3.21	3.34	3.46	3.56	3.67	3.76	3.86	3.94	4.03
	RMSE	1.38	2.09	2.76	3.35	3.89	4.36	4.79	5.18	5.52	5.84	6.12	6.38	6.62	6.84	7.04	7.24	7.42	7.59	7.76	7.92

The bold text in the table is the minimum value of the median for each sample.

4.6. Isotopic Composition

Stable isotopes (δ^{18}O and δ^2H, Table 1) provide insight into the origin of the spring waters and processes in the study area. The δ^{18}O and δ^2H values of the higher temperature thermal CO_2-richwaters range from -14.4% to -18.8% and from -130% to -142%, respectively, those of the lower temperature thermal CO_2-rich waters range from -13.7% to -18.4% and from -127% to -141%, respectively, and those of the shallow groundwaterwere -16.8% and -133%, respectively. The isotopic composition of local precipitation was not measured but was estimated from the Online Isotope in Precipitation Calculator [48] to range from δ^{18}O $= -15.3\%$, δ^2H $= -117.0\%$ at an elevation of 1601 m to δ^{18}O $= -18.5\%$, δ^2H $= -139.0\%$ at an elevation of 3044 m (Figure 12).
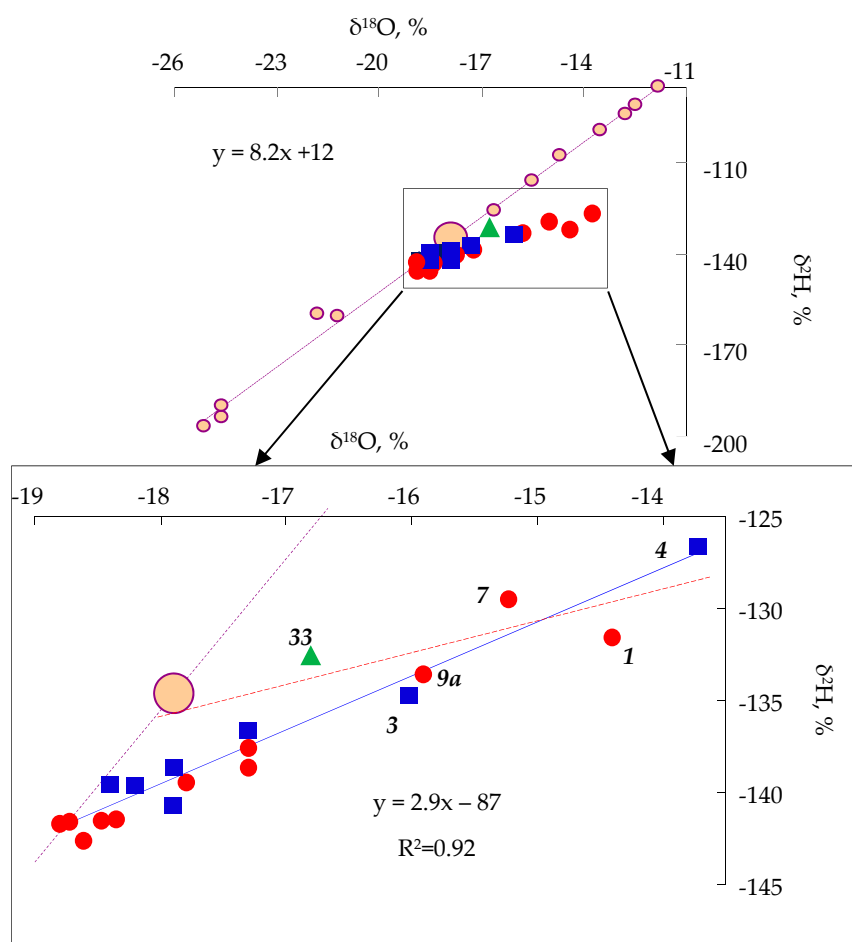
Figure 12. Stable isotopic (δ^{18}O, δ^2H) composition of Group I (higher temperature thermal CO_2-rich waters) (red circles), Group II (lower temperature thermal CO_2-rich waters) (blue squares) and Group III (shallow groundwater) (green triangles) waters compared to that of modelled atmospheric precipitation (pink circles)—monthly (small symbols) and annual (large symbol) along the indicated local meteoric water line (LMWL, equation on diagram). In the magnified inset, the blue line shows the trend line through all the thermal water samples; the red line that through the groundwater and thermal waters (numbers indicate sample numbers) with the maximum shift in δ^{18}O from the LMWL, the slopes of these lines being 2.9 and 1.7, respectively. The isotopic composition of precipitation was calculated using the Online Isotope in Precipitation Calculator [48].

The observed spring water isotopic compositions are broadly consistent with an origin from local precipitation with isotopic enrichment arising from evaporation [49,50]. The intercept of the trend line of the thermal water compositions with the modelled local meteoric water line (LMWL) is slightly

more negative than that of modern meteoric water. This might reflect palaeoclimatic changes, or perhaps more likely, particularly given the observed correlation between spring elevation and $\delta^{18}O$, a relatively high elevation (1600 m to 3100 m; average 2600 m; see Figure 13) of the recharge area of part of the thermal water [1] and might, in part, explain the relatively low slope of the trend line of the thermal water compositions—although other processes, such as isotopic exchange arising from water–rock reactions within the geothermal reservoir [26] cannot be discounted.
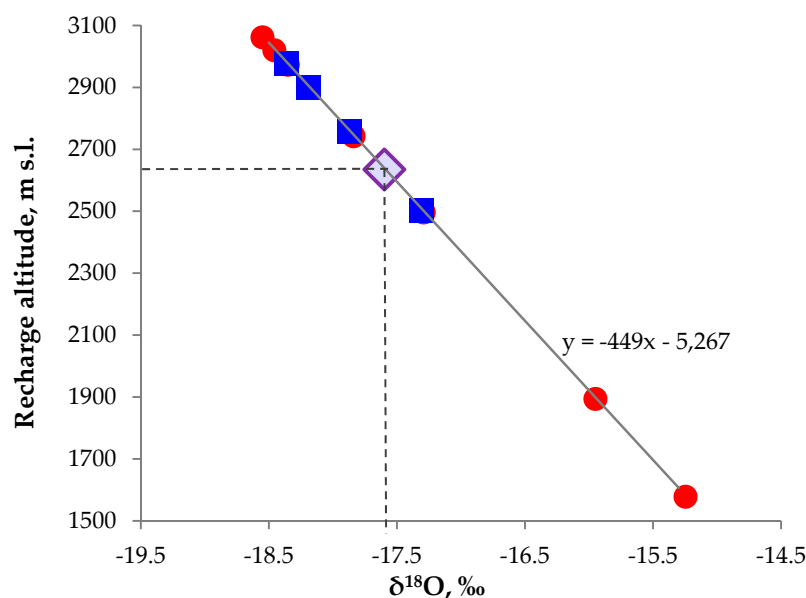
Figure 13. Estimating minimum recharge altitudes of Choygan spring waters. The regression line shows the relationship between altitude and modelled [48] mean $\delta^{18}O$ of local precipitation. This regression line may be used to estimate an altitude of local recharge from the measured $\delta^{18}O$ of the Choygan spring waters (red circles = higher temperature thermal waters (Group I); blue squares = lower temperature thermal waters (Group II), purple diamond = average spring water composition). Inferred enrichment of $\delta^{18}O$ in recharge waters due to evaporative processes means that the values obtained by this method represent minimum recharge altitude estimates.

The wide variation in the mineralogy of the host rocks and the P–T conditions of water–rock interaction in the transit area result in a complex modification of the waters' chemical and isotopic compositions. Fissuring of the geological media causes a mixing of the waters that enter the discharge area from recharge areas with different altitudes (and consequently, flow-path distances).

$\delta^{13}C$ data were used to investigate the source of carbon in the groundwater. The $\delta^{13}C$ (total inorganic dissolved carbon) values observed in the high and low temperature thermal waters samples from springs 5, 10, 11, 13, 15, 18, 19 and 27 were found to range from −0.3 to +1% [51]. Despite the location of springs in a tectonically and seismically active zone with volcanic activity, the presence of large active faults and the presence of mantle helium, the isotopic composition of the CO_2 is consistent with metamorphism of carbonate rocks at depth, although inputs from other sources cannot be ruled out.

4.7. Conceptual Circulation Model

The geological conditions, chemical, gas and isotopic compositions, as well as the estimations of the reservoir temperatures and depths, of the thermal and cold waters make it possible to propose a conceptual circulation model of the origin, the probable types of underground flow paths and the sources of CO_2 in the groundwater of the Choygan natural spa (Figure 14). The appearance of thermal springs is controlled by two factors: the high heat flow in the region (84 MW/m^2) and the presence of

fracture zones that extend to great depths, allowing hot water and CO_2 to quickly rise to the surface. Helium isotope studies of gas and water samples from Choygan (Sample 13) [32] indicate a major (35%) mantle helium component consistent with these elevated heat flows.
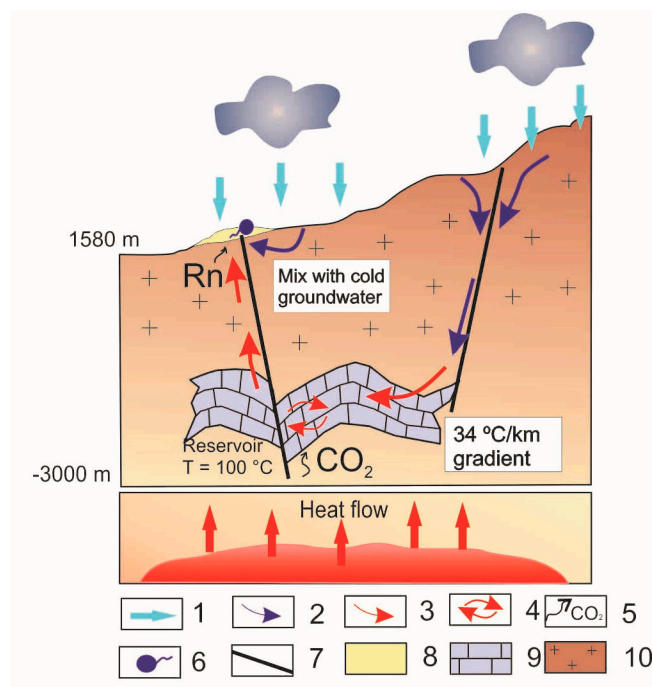

Figure 14. Conceptual model for the geochemical evolution of CO_2-rich springs in the Choygan study area. 1—Rainfall; 2—Groundwater flow; 3—Thermal water flow; 4—Convection; 5—CO_2 flow; 6—Spring; 7—Fault; 8—Travertine; 9—Marbles and limestones; and 10—Granodiorites, plagiogranites and diorites.

The Choygan mineral waters are associated with a large E–W striking fault in the Precambrian rocks (plagiogranites, diorites and granodiorites) intruded by Paleozoic granites and diorites. The isotopic composition of these waters reflects their meteoric origin as well as evaporative processes and perhaps also isotopic exchange during water–rock reactions.

Atmospheric precipitation having ambient surface temperatures infiltrates the ground presumably at high altitudes, between about 1600 m and 3000 m (cf. Topographer's Peak, height of 3044 m above sea level, see Figure 1) and percolates, including through faults and other higher permeability structures into the hydrogeological system, where it reacts with primary aluminosilicate minerals that are not in equilibrium with the waters. These reactions result in non-stoichiometric dissolution, particularly silicate minerals inplagiogranites, diorites, schists andgneiss. The water reaches saturation with respect to kaolinite and montmorillonite and carbonate minerals are precipitated, with a concomitant net increase in Na, K, Ca, Mg and TDS. Palaeozoic metamorphics, particularly including highly faulted and fractured marbles and limestones may be the reservoir units supplying CO_2 for the Choygan thermal springs. The reservoir temperature of water reaches up to approximately 100 °C at a depth of nearly 3 km.

After heating at depth, water rises via major faults toward the surface, accompanied by mixing with cooler, variably more oxidizing groundwaters, and ultimately discharging at the surface, with concomitant precipitation of carbonates (notably travertine), Fe(III)-O-H phases and admixture with air. Radon produced by radioactive decay of Ra-226 originating from uranium-enriched felsic rocks is incorporated into the waters relatively close to the discharge zones.

5. Conclusions

Thermal CO_2-rich mineral waters in the Eastern Sayan Mountainous area in East Tuva (Russia) as exemplified by springs discharging around the Choygan mineral water natural spa, range in composition from higher temperature HCO_3–Na–Ca type waters to lower temperature HCO_3–Ca–Na type waters and broadly represent mixing between higher Na/Ca geothermal waters and higher Ca/Na near surface groundwaters. All springs emerge along faults, which have the potential to transmit waters rapidly from great depths.

Although mixing appears to be the dominant process controlling major element hydrogeochemistry, the non-conservative behaviour of CO_2 and SO_4 may reflect degassing and/or other processes. All the waters are ultimately of meteoric origin with stable isotopic signatures reflecting recharge from colder environments than that of the modern day discharge areas and isotopic fractionation during evaporative processes. Mixing processes result in water compositions that are strongly out of equilibrium with Na-K-Ca phases; accordingly, the most reliable estimates of geothermal reservoir temperatures are obtained from silica geothermometry and an analysis of temperature-dependent convergence of likely reservoir mineral saturation indices—these suggest reservoir temperatures of around 80 to 100 °C consistent with a previously observed geothermal gradient in the area of around 34 °C/km and a reservoir depth of approximately 3 km.

Future research on determining the isotopic composition of local surface waters (rivers, precipitation, shallow groundwater) as well as more extensive measurements of $\delta^{13}C$ and $\delta^{18}O$ are recommended to provide a better understanding of the origin of variable CO_2 concentraions, and in particular to better discriminated between degassing, oxidation and mixing processes in controlling the chemical compositions of these thermal waters.

Conflicts of Interest: The authors declare no conflicts of interest.

References

1. Sharifi, R.; Moore, F.; Mohammadi, Z.; Keshavarzi, B. Estimation of deepwater temperature and hydrogeochemistry of springs in the Takab geothermal field, West Azerbaijan, Iran. *Environ. Monit. Assess.* **2016**, *188*, 75. [CrossRef] [PubMed]

2. Afsin, M.; Allen, D.M.; Kirste, D.; Durukan, U.G.; Gurel, A.; Oruc, O. Mixing processes in hydrothermal spring systems and implications for interpreting geochemical data: A case study in the Cappadocia region of Turkey. *Hydrogeol. J.* **2014**, *22*, 7–23. [CrossRef]

3. Alcicek, H.; Bulbul, A.; Alcicek, M.C. Hydrogeochemistry of the thermal waters from the Yenice Geothermal Field (Denizli Basin, Southwestern Anatolia, Turkey). *J. Volcanol. Geotherm. Res.* **2016**, *309*, 118–138. [CrossRef]

4. Mohammadi, Z.; Parizi, H.S. Hydrogeochemistry and geothermometry of the Jowshan thermal springs, Central Iran. *Geochem. Int.* **2013**, *51*, 994–1004. [CrossRef]

5. Todorović, M.; Marina, J.Š.; Ćuk, J.A.; Šišović, J. Mineral and Thermal Waters of Serbia: Multivariate Statistical Approach to Hydrochemical Characterization. Environ. *Earth Sci.* **2015**, 81–95. [CrossRef]

6. Pantic, T.P.; Birke, M.; Petrovic, B.; Nikolov, J.; Dragisic, V.; Zivanovic, V. Hydrogeochemistry of thermal groundwaters in the Serbian crystalline core region. *J. Geochem. Explor.* **2015**, *159*, 101–114. [CrossRef]

7. Andolssi, M.; Alyahyaoui, S.; Makni, J.; Charef, A.; Zouari, H.; Tarki, M.; Challouf, B. Integrated study of surface and subsurface data for prospecting hydrogeothermal basins of hot water spring Ain El Hammam: Case of Utique region basin (extreme north of Tunisia). *Arab. J. Geosci.* **2015**, *8*, 8879–8897. [CrossRef]

8. Brahim, B.; Makni, F.J.; Bouri, S.; Ben Dhia, H. Evaluation of temperature and mixing process of water in deep and shallow aquifers in the Southwestern Tunisia: Case of Djerid Region. *Arab. J Sci. Eng.* **2014**, *39*, 5677–5689. [CrossRef]

9. Pandarinath, K.; Domínguez-Domínguez, H. Evaluation of the solute geothermometry of thermal springs and drilled wells of La Primavera (Cerritos Colorados) geothermal field, Mexico: A geochemometrics approach. *J. South Am. Earth Sci.* **2015**, *62*, 109–124. [CrossRef]

10. Wurl, J.; Mendez Rodriguez, L.C.; Cassassuce, F.; Martinez Gutierrez, G.; Ramos Velazquez, E. Geothermal water in the San Juan Bautista Londo aquifer, BCS, Mexico. *Proc. Earth Planet. Sci.* **2013**, *7*, 900–903. [CrossRef]

11. Guo, Q.; Liu, M.; Li, J.; Zhang, X.; Wang, Y. Acid hot springs discharged from the Rehai hydrothermal system of the Tengchong volcanic area (China): Formed via magmatic fluid absorption or geothermal steam heating? *Bull. Volcanol.* **2014**, *76*, 868. [CrossRef]

12. Xiangquan, L.; Xinwei, H.; Zhichao, Z.; Lingxia, L. Geochemical characterization and origins of the thermal springs in southern Gaoligong Mountains, China. Environ. *Earth Sci.* **2014**, *72*, 3089–3098. [CrossRef]

13. Koh, Y.-K.; Choi, B.-Y.; Yun, S.-T.; Hyeon-Su, C.C.; Mayer, B.; Ryoo, S.-W. Origin and evolution of two contrasting thermal groundwaters (CO_2-rich and alkaline) in the Jungwon area, South Korea: Hydrochemical and isotopic evidence. *J. Volcanol. Geotherm. Res.* **2008**, *178*, 777–786. [CrossRef]

14. Choi, H.-S.; Yun, S.-T.; Koh, Y.-K.; Mayer, B.; Park, S.-S.; Hutcheon, I. Geochemical behavior of rare earth elements during the evolution of CO_2-rich groundwater: A study from the Kangwon district, South Korea. *Chem. Geol.* **2009**, *262*, 318–327. [CrossRef]

15. Choi, B.Y.; Yun, S.T.; Kim, K.H.; Choi, H.S.; Chae, G.T.; Lee, P.K. Geochemical modeling of CO_2-water–rock interactions for two different hydrochemical types of CO_2-rich springs in Kangwon District, Korea. *J. Geochem. Explor.* **2014**, *144*, 49–62. [CrossRef]

16. Marques, J.M.; Monteiro Santos, F.A.; Graça, R.C.; Castro, R.; Aires-Barros, L.; Mendes Victor, L.A. A geochemical and geophysical approach to derive a conceptual circulation model of CO_2-rich mineral waters: A case study of Vilarelho da Raia, northern Portugal. *J. Hydrogeol.* **2001**, *9*, 584–596. [CrossRef]

17. Cruz, J.V.; Freire, P.; Costa, A. Mineral waters characterization in the Azores archipelago (Portugal). *J. Volcanol. Geotherm. Res.* **2010**, *190*, 353–364. [CrossRef]

18. Corral, M.M.; Galindo, E.; Ontiveros, C.; Munoz, J.A.D. Hydrogeochemical areas as background for specific mineral and thermal waters of Spain. Environ. *Earth Sci.* **2015**, *73*, 2683–2697. [CrossRef]

19. Molli, G.; Doveri, M.; Manzella, A.; Bonin, L.; Botti, F.; Menichini, M.; Montanari, D.; Trumpy, E.; Ungari, A.; Vaselli, L. Surface-subsurface structural architecture and groundwater flow of the EquiTerme hydrothermal area, northern Tuscany Italy. *Ital. J. Geosci.* **2015**, *134*, 442–457. [CrossRef]

20. Dewandel, B.; Alazard, M.; Lachassagne, P.; Bailly-Comte, V.; Couëffé, R.; Grataloup, S.; Ladouche, B.; Lanini, S.; Maréchal, J.C.; Wyns, R. Respective roles of the weathering profile and the tectonic fractures in the structure and functioning of crystalline thermomineral carbo-gaseous aquifers. *J. Hydrol.* **2017**, *547*, 690–707. [CrossRef]

21. Maréchal, J.C.; Lachassagne, P.; Ladouche, B.; Dewandel, B.; Lanini, S.; Le Strat, P.; Petelet-Giraud, E. Structure and hydrogeochemical functioning of a sparkling natural mineral water system determined using a multidisciplinary approach: A case study from southern France. *Hydrogeol. J.* **2014**, *22*, 47–68. [CrossRef]

22. El-Fiky, A.A. Hydrogeochemistry and geothermometry of thermal groundwater from the Gulf of Suez Region, Egypt JKAU. *Earth Sci.* **2009**, *20*, 71–96.

23. El-Rayes, A.E.; Arnous, M.O.; Aboulela, H.A. Hydrogeochemical and seismological exploration for geothermal resources in South Sinai, Egypt utilizing GIS and remote sensing. *Arab. J. Geosci.* **2015**, *8*, 5631–5647. [CrossRef]

24. Chelnokov, G.; Kharitonova, N.; Bragin, I.; Chudaev, O. Geochemistry of mineral water and gases of the Razdolnoe Spa (Primorye, Far East of Russia). *Appl. Geochem.* **2015**, *59*, 147–154. [CrossRef]

25. Zamana, L.V.; Askarov, S.A.; Borzenko, S.V.; Chudaev, O.V.; Bragin, I.V. Isotopes of sulfide and sulfate sulfur in nitrogen hot springs of the bauntov group (Baikal Rift Zone). *Dokl. Earth Sci.* **2010**, *435*, 1515–1517. (In Russian) [CrossRef]

26. Kopylova, Y.G.; Guseva, N.V.; Khvashchevskaya, A.A.; Arakchaa, K.D. Geochemistry of carbon dioxide mineral waters of the Choigan natural complex (northeastern Tuva). *Russ. Geol. Geophys.* **2014**, *55*, 1295–1305. [CrossRef]

27. Kopylova, Y.; Guseva, N.; Shestakova, A.; Khvaschevskaya, A.; Arakchaa, K. Dissolved gas composition of groundwater in the natural spa complex "Choygan mineral waters" (East Tuva). *J. IOP Conf. Ser. Earth Environ. Sci.* **2014**, *21*, 012022. [CrossRef]

28. Kopylova, Y.G.; Guseva, N.V.; Shestakova, A.V.; Khvashchevskaya, A.A.; Arakchaa, K.D. Uranium and thorium behavior in groundwater of the natural spa area "Choygan mineral water" (East Tuva). *J. IOP Conf. Ser. Earth Environ. Sci.* **2015**, *21*, 012034. [CrossRef]

29. Shestakova, A.V. Investigation of natural mineral waters of Choigan complex (Eastern Tyva). Problems of Geology and Subsurface Development. In Proceedings of the 18th International Symposium in Honour of Academician M. A. Usov, Tomsk, Russia, 7–11 April 2014; TPU Publishing House: Tomsk, Russia, 2014.

30. Badminov, P.S.; Ivanov, A.V.; Pisarskii, B.I.; Orgilyanov, A.I. The Oka hydrothermal system, East Sayan Mountains. *J. Volcanol. Seismol.* **2013**, *7*, 265–276. (In Russian) [CrossRef]

31. Shestakova, A.V.; Guseva, N.V. Calculation of deep temperatures of thermal waters in Eastern Tuva. *Bull. Tomsk Polytech. Univ. Geo Assets Eng.* **2018**, *329*, 25–36. (In Russian)

32. Duchkov, A.; Rychkova, K.; Lebedev, V.; Kamensky, I.; Sokolova, L. Estimation of heat flow in Tuva from data on helium isotopes in thermal mineral springs. *Russ. Geol. Geophys.* **2010**, *51*, 264–276. [CrossRef]

33. Gemici, U.; Tarcan, G. Hydrogeochemistry of the Hisarkoy geothermal area (Balikesir) Western Turkey. In Proceedings of the 12th International Symposium on Water-Rock Interaction, WRI-12, Kunming, China, 31 July–5 August 2007. [CrossRef]

34. Weather Base. Weather in Orlik, Russia. Available online: http://www.weatherbase.com/weather/weather.php3?s=99992&cityname=Orlik%2C+Khabarovsk+Krai%2C+Russia&units= (accessed on 7 April 2018).

35. Galimova, T.F.; Pashkova, A.G.; Povarintseva, S.A.; Perfiliev, V.V. *State Geological Map of the Russian Federation*; Scale 1: 1 Million (Third Generation); Angara-Yenisei Series; Sheet N-47; Cartographic Factory VSEGEI: St. Petersburg, Russia, 2012. (In Russian)

36. Zuev, V. Portable field syringe degasser. In *Multipurpose Hydrogeochemical Study in Connection with the Search for Mineral Resources and the Protection of Groundwater*; TPU: Tomsk, Russia, 1993; pp. 185–186. (In Russian)

37. Verma, S.P.; Pandarinath, K.; Santoyo, E. Sol Geo: A new computer program for solute geothermometers and its application to Mexican geothermal fields. *J. Geotherm.* **2008**, *37*, 597–621. [CrossRef]

38. Bethke, C.M. *Geochemical Reaction Modeling, Concepts and Applications*; Oxford University Press: New York, NY, USA, 1996; 416p, ISBN 0195094751.

39. Reed, M.H.; Spycher, N. Calculation of pH and mineral equilibria in hydrothermal waters with application to geothermometry and studies of boiling and dilution. *Geochim. Cosmochim. Acta.* **1984**, *48*, 1479–1492. [CrossRef]

40. Spycher, N.; Peiffer, L.; Sonnenthal, E. *GeoT User's Guide, a Computer Program for Multicomponent Geothermometry and Geochemical Speciation*; Lawrence Berkeley Natl. Lab.: Berkeley, CA, USA, 2014; pp. 1–38.

41. Kralj, P. Rare Earth Elements in Thermal Water from the Sob-1 Well, MurskaSobota, NE Slovenia. *Environ. Earth Sci.* **2009**, *59*, 5–13. [CrossRef]

42. Belhai, M.; Fujimitsu, Y.; Bouchareb-Haouchine, Z.F.; Iwanaga, T.; Noto, M.; Nishijima, J. Hydrogeochemical and isotope geochemical study of northwestern Algerian thermal waters. *Arab. J. Geosci.* **2016**, *35*, 271–287. [CrossRef]

43. Lavrushin, V. *Subsurface Fluids of the Greater Caucasus and Its Surrounding*; GEOS: Moscow, Russia, 2012; Volume 599, p. 348. ISBN 978-5-89118-579-1. (In Russian)

44. Bonotto, D.M. 222Rn, 220Rn and other dissolved gases in mineral waters of southeast Brazil. *J. Environ. Radioact.* **2014**, *132*, 21–30. [CrossRef] [PubMed]

45. Shivakumara, B.C.; Chandrashekara, M.S.; Kavitha, E.; Paramesh, L. Studies on 226Ra and 222Rn concentration in drinking water of Mandya region, Karnataka State, India. *J. Radiat. Res. Appl. Sci.* **2014**, *7*, 491–498. [CrossRef]

46. Giggenbach, W.F.; Werner, F. Geothermal solute equilibria. Derivation of Na-K-Mg-Ca geoindicators. *Geochim. Cosmo. Acta* **1988**, *52*, 2749–2765. [CrossRef]

47. Kaszuba, J.; Yardley, B.; Andreani, M. Experimental perspectives of mineral dissolution and precipitation due to carbon dioxide-water–rock interactions. *Rev. Mineral. Geochem.* **2013**, *77*, 153–188. [CrossRef]

48. The Online Isotopes in Precipitation Calculator. Available online: http://wateriso.utah.edu/waterisotopes/pages/data_access/oipc.html (accessed on 7 April 2018).

49. Bowen, G.J.; Wassenaar, L.I.; Hobson, K.A. Global application of stable hydrogen and oxygen isotopes to wildlife forensics. *Oecologia* **2005**, *143*, 337–348. [CrossRef] [PubMed]

50. Başaran, C.; Gökgöz, A. Hydrochemical and isotopic properties of Heybeli geothermal area (Afyon, Turkey). *Arab. J. Geosci.* **2016**, *9*, 586. [CrossRef]

51. Orgilyanov, A.; Kryukova, I.; Badminov, P. Medical carbonated mineral water of Mongolian-Baikal region. *Spa Base Nat. Ther. Areas Tuva Adjac. Reg.* **2015**, *2*, 103–108. (In Russian)